Supplement of Atmos. Chem. Phys., 25, 4719–4753, 2025
https://doi.org/10.5194/acp-25-4719-2025-supplement
© Author(s) 2025. CC BY 4.0 License.

Atmospheric Chemistry and Physics
Open Access

Supplement of

A comprehensive global modeling assessment of nitrate heterogeneous formation on desert dust

Rubén Soussé Villa et al.

Correspondence to: Rubén Soussé Villa (ruben.sousse@bsc.es) and Oriol Jorba (oriol.jorba@bsc.es)

The copyright of individual parts of the supplement might differ from the article licence.

S1 Model emissions, size bins and alkalinity calculations

Table S1. Total emissions (anthropogenic, biogenic and biomass burning) for 2018 used in this study.

Species	**Emission (Tgy-1)**
NO	75.93
NO2	17.86
HONO	0.51
NH3	61.81
SO2	104.40
PM2.5SO4	0.53

Table S2: Density, volumetric radius, effective radius, pm2.5 and pm10 fractions of each bin of the studied species.

				DUST					
	units	**bin 1**	**bin 2**	**bin 3**	**bin 4**	**bin 5**	**bin 6**	**bin 7**	**bin 8**
Density	kgm-3	2500	2500	2500	2500	2650	2650	2650	2650
Radius vol.	μm	0.15	0.25	0.47	0.8	1.36	2.29	3.93	7.24
Radius eff.	μm	0.15	0.25	0.45	0.78	1.32	2.24	3.80	7.11
PM2.5 frac.		1	1	1	1	0.38	0	0	0
PM10 frac.		1	1	1	1	1	1	0.87	0
				SEA_SALT					
	units	**bin 1**	**bin 2**	**bin 3**	**bin 4**	**bin 5**	**bin 6**	**bin 7**	**bin 8**
Density	kgm-3	2160	2160	2160	2160	2160	2160	2160	2160
Radius vol.	μm	0.15	0.25	0.47	0.81	1.40	2.37	4.30	9.23
Radius eff.	μm	0.14	0.24	0.45	0.79	1.36	2.32	4.13	8.64
PM2.5 frac.		1	1	1	1	0.32	0	0	0
PM10 frac.		1	1	1	1	1	1	0.75	0
				NO3					
	units	**bin 1**	**bin 2**						
Density	kgm-3	1700	2380						
Radius vol.	μm	0.35	2.23						
Radius eff.	μm	0.24	1.79						
PM2.5 frac.		1	0.2						
PM10 frac.		1	1						
				NH4					
	units	**bin 1**	**bin 2**						
Density	kgm-3	1700	2380						
Radius vol.	μm	0.35	2.23						
Radius eff.	μm	0.24	1.79						
PM2.5 frac.		1	0.2						
PM10 frac.		1	1						
				SO4					
	units	**bin 1**	**bin 2**						
Density	kgm-3	1700	2380						
Radius vol.	μm	0.35	2.23						
Radius eff.	μm	0.24	1.79						
PM2.5 frac.		1	0.2						
PM10 frac.		1	1						

Mineral	Bin 1	Bin 2	Bin 3	Bin 4	Bin 5	Bin 6	Bin 7	Bin 8	Soluble in water?	Soluble in acids?	Assumed reactive?	Notes/ References
Illite	8.5E-5	4.1E-4	3.1E-3	8.8E-3	2.2E-2	3.2E-2	5.5E-2	1.4E-2	no	yes	yes	1
Montmorillonite	6.2E-5	3.0E-4	2.2E-3	6.4E-3	1.6E-2	2.3E-2	4.0E-2	1.0E-2	-	yes	yes	2
Kaolinite	7.8E-5	3.7E-4	2.8E-3	8.0E-3	2.0E-2	2.9E-2	5.0E-2	1.3E-2	no	yes	no	3
Chlorite	1.2E-5	5.6E-5	4.2E-4	1.2E-3	4.8E-3	1.1E-2	2.6E-2	7.9E-3	no	-	no	4
Vermiculite	7.9E-6	3.8E-5	2.8E-4	8.1E-4	2.1E-3	2.9E-3	5.1E-3	1.3E-3	no	no	no	5
Feldspar	3.4E-6	1.6E-5	1.2E-4	3.5E-4	6.3E-3	2.2E-2	6.0E-2	1.9E-2	no	yes	yes	6
Quartz	1.2E-5	5.8E-5	4.4E-4	1.3E-3	1.9E-2	6.6E-2	1.8E-1	5.6E-2	no	no	no	7
Calcite	3.1E-5	1.5E-4	1.1E-3	3.2E-3	1.0E-2	1.9E-2	3.9E-2	1.1E-2	yes	yes	yes	8
Hematite	3.5E-6	1.7E-5	1.3E-4	3.6E-4	9.2E-4	1.3E-3	2.3E-3	5.9E-4	no	yes	no	9
Goethite	6.2E-6	2.9E-5	2.2E-4	6.3E-4	1.8E-3	3.1E-3	6.2E-3	1.8E-3	no	-	no	10
Gypsum	4.7E-7	2.2E-6	1.7E-5	4.8E-5	1.4E-4	2.5E-4	5.2E-4	1.5E-4	poor	yes	no	11
Mica	0.0E+0	0.0E+0	0.0E+0	0.0E+0	2.7E-3	1.0E-2	2.8E-2	9.0E-3	no	no	no	12
Total	3.0E-4	1.4E-3	1.1E-2	3.1E-2	1.1E-1	2.2E-1	4.9E-1	1.5E-1				

Table S3. Globally-averaged fractions (0 to 1) of the minerals attributed to each bin from the Journet et al. (2014) mineral database. The respective references for the assumed solubility of each mineral are:

1. Assumed reactive because relatively soluble in acids (Webmineral, 2008f)
2. Assumed reactive because relatively soluble in acids (Nutting, 1941, 1932)
3. Assumed nonreactive because predominantly containing Al and Si (Yang, 2008).
4. Assumed nonreactive because not soluble in water (Britannica, The Editors of Encyclopaedia, 2018; Mindat.org, a).
5. Assumed nonreactive because not soluble (Huggett, 2015; Schulze, 2005; Bleam, 2017).
6. Assumed reactive because relatively soluble in acids (Blum, 1994; Mindat.org, b).
7. Assumed nonreactive because not soluble (Usher et al., 2003).
8. Assumed reactive because highly soluble (Usher et al., 2003; Krueger et al., 2004; Hodzic et al., 2006).
9. Assumed nonreactive because iron is not considered in ISORROPIA-II (National Center for Biotechnology Information, 2024a; Weast, 1980).
10. Assumed nonreactive because not soluble, although lacking information if soluble in acids. (Essington et al., 2005; National Center for Biotechnology Information. PubChem Compound Database, 2024b).
11. Assumed nonreactive because poorly soluble in water and soluble only in high acidity solutions (Zhang and Muhammed, 1989; National Center for Biotechnology Information. PubChem Compound Database, 2024a; Krueger et al., 2004; Hodzic et al., 2006).
12. Assumed nonreactive because non soluble (National Center for Biotechnology Information, 2024b).

Mineral	Mineral Mw (g/mol)	Soluble element	Element Mw (g/mol)	Element fraction	Bin 1	Bin 2	Bin 3	Bin 4	Total fine	Bin 5	Bin 6	Bin 7	Bin 8	Total coarse	Total	References
Illite	389.34	K	39.10	0.10	2.84%	2.84%	2.84%	2.84%	2.84%	2.10%	1.45%	1.13%	0.99%	1.41%	2.20%	1
	389.34	Mg	24.31	0.06	1.76%	1.76%	1.76%	1.76%	1.76%	1.30%	0.90%	0.70%	0.62%	0.88%	1.37%	1
Montmorillonite	549.07	Ca	40.08	0.07	1.50%	1.50%	1.50%	1.50%	1.50%	1.11%	0.76%	0.59%	0.52%	0.75%	1.16%	2
	549.07	Na	22.99	0.04	0.86%	0.86%	0.86%	0.86%	0.86%	0.63%	0.44%	0.34%	0.30%	0.43%	0.67%	2
Feldspar																
- 1/3 Albite	263.02	Na (1/3)	22.99	0.03	0.03%	0.03%	0.03%	0.03%	0.03%	0.16%	0.27%	0.32%	0.35%	0.27%	0.14%	3
- 1/3 Anorthite	277.41	Ca (1/3)	40.08	0.04	0.05%	0.05%	0.05%	0.05%	0.05%	0.26%	0.44%	0.53%	0.57%	0.45%	0.23%	4
- 1/3 Orthoclase	278.33	K (1/3)	39.10	0.04	0.05%	0.05%	0.05%	0.05%	0.05%	0.25%	0.43%	0.52%	0.56%	0.44%	0.22%	5
Calcite	100.09	Ca	40.08	0.40	4.15%	4.15%	4.15%	4.15%	4.15%	3.76%	3.41%	3.23%	3.16%	3.39%	3.81%	6
Gypsum	172.20	Ca	40.08	0.23	0.04%	0.04%	0.04%	0.04%	0.04%	0.03%	0.03%	0.02%	0.02%	0.03%	0.03%	7
Total Ca					5.73%	5.73%	5.73%	5.73%	**5.73%**	5.15%	4.64%	4.39%	4.28%	**4.61%**	**5.17%**	
Total Na					0.89%	0.89%	0.89%	0.89%	**0.89%**	0.79%	0.71%	0.66%	0.65%	**0.70%**	**0.79%**	
Total K					2.88%	2.88%	2.88%	2.88%	**2.88%**	2.35%	1.88%	1.64%	1.55%	**1.85%**	**2.37%**	
Total Mg					1.76%	1.76%	1.76%	1.76%	**1.76%**	1.30%	0.90%	0.70%	0.62%	**0.88%**	**1.32%**	

Table S4. The NVC content from globally-averaged mineralogy of Journet et al. (2014) assumed for each size bin, derived from those minerals assumed to be soluble in water (Supplementary Table S3). The respective references for the ionic composition of each mineral and molar masses are:

1. Webmineral (2008f)
2. Nutting (1941, 1932)
3. Webmineral (2008a)
4. Webmineral (2008b)
5. Webmineral (2008e)
6. Webmineral (2008c); National Center for Biotechnology Information. PubChem Compound Database (2024a)
7. Webmineral (2008d); Hulett and Allen (1902)

Mineral	Bin 1	Bin 2	Bin 3	Bin 4	Bin 5	Bin 6	Bin 7	Bin 8	Soluble in water?	Soluble in acids?	Assumed reactive?	Notes/ References
Illite	1.1E-04	5.4E-04	4.0E-03	1.2E-02	2.9E-02	4.2E-02	7.2E-02	1.9E-02	no	yes	yes	1
Montmorillonite	6.4E-05	3.0E-04	2.3E-03	6.5E-03	1.7E-02	2.4E-02	4.1E-02	1.1E-02	-	yes	yes	2
Kaolinite	7.6E-05	3.6E-04	2.7E-03	7.8E-03	2.0E-02	2.8E-02	4.8E-02	1.3E-02	no	yes	no	3
Calcite	1.3E-05	6.3E-05	4.7E-04	1.4E-03	5.2E-03	1.2E-02	2.7E-02	8.0E-03	yes	yes	yes	4
Quartz	2.0E-05	9.7E-05	7.3E-04	2.1E-03	2.4E-02	8.0E-02	2.1E-01	6.7E-02	no	no	no	5
Feldspar	8.1E-06	3.9E-05	2.9E-04	8.3E-04	8.5E-03	2.8E-02	7.3E-02	2.3E-02	no	yes	yes	6
Iron Oxide	4.6E-06	2.2E-05	1.6E-04	4.7E-04	1.6E-03	3.3E-03	7.3E-03	2.2E-03	-	-	no	7
Gypsum	3.4E-06	1.6E-05	1.2E-04	3.5E-04	1.3E-03	2.8E-03	6.3E-03	1.9E-03	poor	yes	no	8
Total	3.0E-04	1.4E-03	1.1E-02	3.1E-02	1.1E-01	2.2E-01	4.9E-01	1.4E-01				

Table S5. Globally-averaged fractions (0 to 1) of the minerals attributed to each bin from the Claquin et al. (1999) mineral database. The respective references for the assumed solubility of each mineral are: References:

1. Assumed reactive because relatively soluble in acids (Webmineral, 2008f).
2. Assumed reactive because relatively soluble in acids (Nutting, 1941, 1932).
3. Assumed nonreactive because predominantly containing Al and Si (Yang, 2008).
4. Assumed reactive because highly soluble (Usher et al., 2003; Krueger et al., 2004; Hodzic et al., 2006).
5. Assumed nonreactive because not soluble (Usher et al., 2003).
6. Assumed reactive because relatively soluble in acids (Blum, 1994; Mindat.org, b).
7. Assumed nonreactive because iron is not considered in ISORROPIA-II (National Center for Biotechnology Information, 2024a; Weast, 1980).
8. Assumed nonreactive because poorly soluble in water and soluble only in high acidity solutions (Zhang and Muhammed, 1989; National Center for Biotechnology Information. PubChem Compound Database, 2024a; Krueger et al., 2004; Hodzic et al., 2006).

Mineral	Mineral Mw (g/mol)	Soluble element	Element Mw (g/mol)	Element fraction	Bin 1	Bin 2	Bin 3	Bin 4	Total fine	Bin 5	Bin 6	Bin 7	Bin 8	Total coarse	Total	References
Illite	389.340	K	39.10	0.10	3.76%	3.76%	3.76%	3.76%	3.76%	2.78%	1.92%	1.49%	1.31%	1.88%	2.92%	1
	389.340	Mg	24.31	0.06	2.34%	2.34%	2.34%	2.34%	2.34%	1.73%	1.19%	0.93%	0.82%	1.17%	1.82%	1
Montmorillonite	549.070	Ca	40.08	0.07	1.54%	1.54%	1.54%	1.54%	1.54%	1.14%	0.78%	0.61%	0.54%	0.77%	1.20%	2
	549.070	Na	22.99	0.04	0.88%	0.88%	0.88%	0.88%	0.88%	0.65%	0.45%	0.35%	0.31%	0.44%	0.69%	2
Feldspar																
- 1/3 Albite	263.020	Na (1/3)	22.99	0.03	0.07%	0.07%	0.07%	0.07%	0.07%	0.21%	0.33%	0.39%	0.42%	0.34%	0.19%	3
- 1/3 Anorthite	277.410	Ca (1/3)	40.08	0.04	0.12%	0.12%	0.12%	0.12%	0.12%	0.35%	0.55%	0.65%	0.70%	0.56%	0.31%	4
- 1/3 Orthoclase	278.330	K (1/3)	39.10	0.04	0.11%	0.11%	0.11%	0.11%	0.11%	0.34%	0.54%	0.63%	0.68%	0.55%	0.31%	5
Calcite	100.090	Ca	40.08	0.40	1.76%	1.76%	1.76%	1.76%	1.76%	1.95%	2.11%	2.19%	2.22%	2.12%	1.92%	6
Gypsum	172.200	Ca	40.08	0.23	0.26%	0.26%	0.26%	0.26%	0.26%	0.28%	0.30%	0.30%	0.31%	0.30%	0.28%	7
Total Ca					3.68%	3.68%	3.68%	3.68%	**3.68%**	3.71%	3.74%	3.76%	3.76%	**3.74%**	**3.71%**	
Total Na					0.95%	0.95%	0.95%	0.95%	**0.95%**	0.86%	0.78%	0.75%	0.73%	**0.78%**	**0.87%**	
Total K					3.87%	3.87%	3.87%	3.87%	**3.87%**	3.12%	2.45%	2.13%	1.99%	**2.42%**	**3.15%**	
Total Mg					2.34%	2.34%	2.34%	2.34%	**2.34%**	1.73%	1.19%	0.93%	0.82%	**1.17%**	**1.75%**	

Table S6. The NVC content from globally-averaged mineralogy of Journet et al. (2014) assumed for each size bin, derived from those minerals assumed to be soluble in water (Supplementary Table S5). The respective references for the ionic composition of each mineral and molar masses are:

1. Webmineral (2008f)
2. Nutting (1941, 1932)
3. Webmineral (2008a)
4. Webmineral (2008b)
5. Webmineral (2008e)
6. Webmineral (2008c); National Center for Biotechnology Information. PubChem Compound Database (2024a)
7. Webmineral (2008d); Hulett and Allen (1902)

S2 Spatial distributions

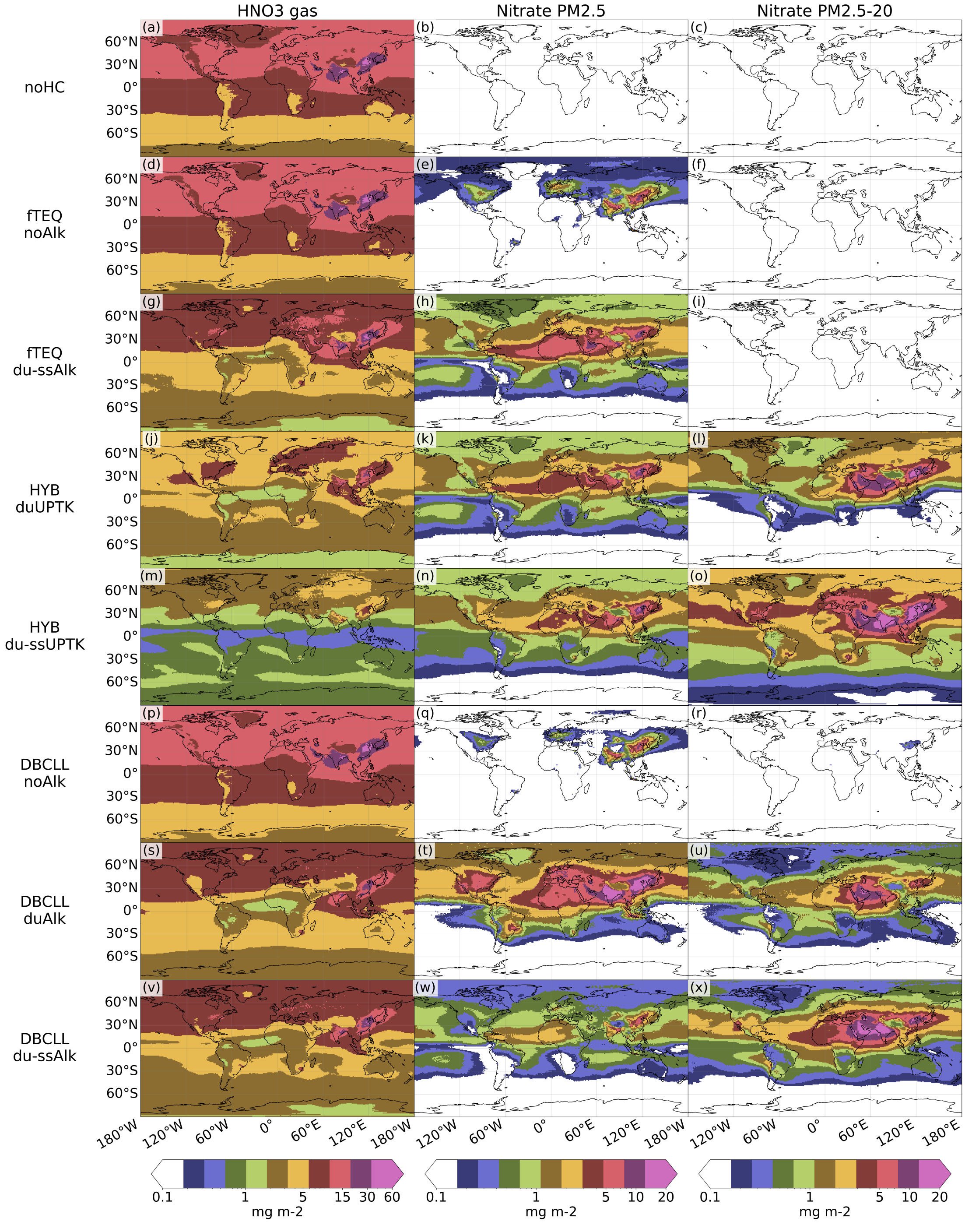

Figure S1. Column loads ($mg\ m^{-2}$) of $HNO_{3(g)}$, fine and coarse particulate nitrate simulated by the different mechanisms, averaged for 2018.

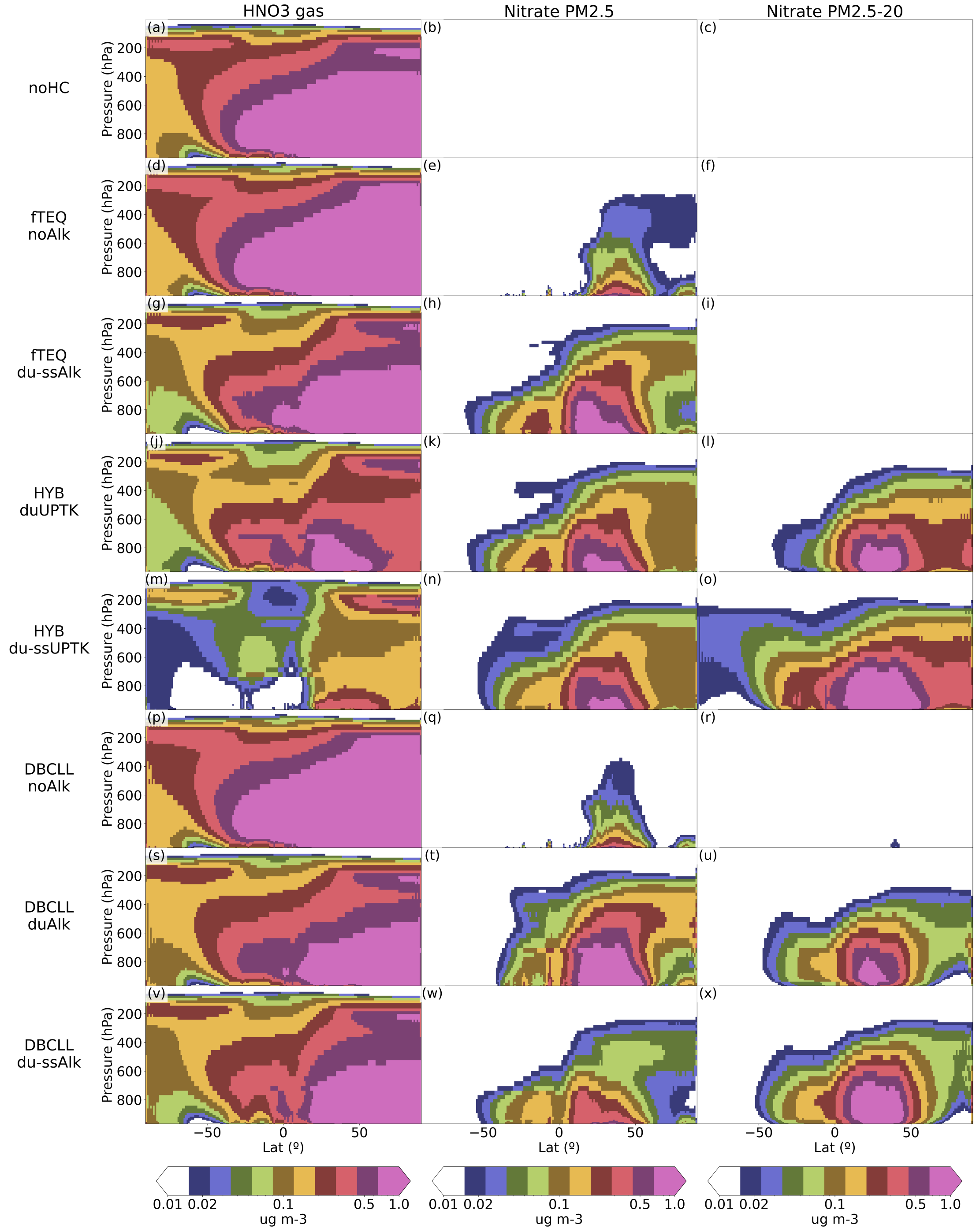

Figure S2. Zonal average concentrations ($\mu g\ m^{-3}$) of HNO_3, fine and coarse particulate nitrate simulated by the different mechanisms, averaged for 2018.

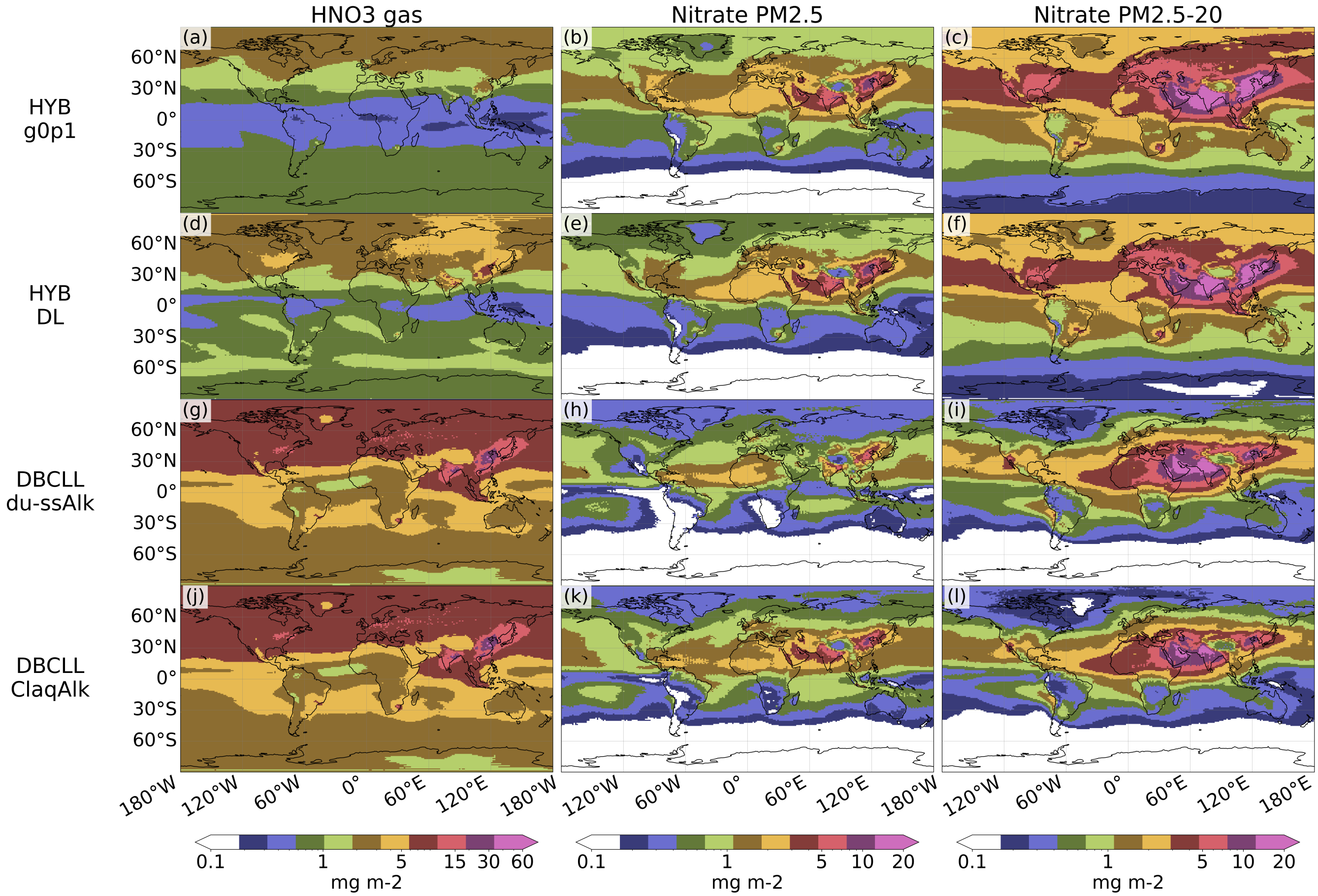

Figure S3. Column loads ($mg\, m^{-2}$) of $\mathrm{HNO_{3(g)}}$, fine and coarse particulate nitrate simulated by additional mechanisms, averaged for 2018.

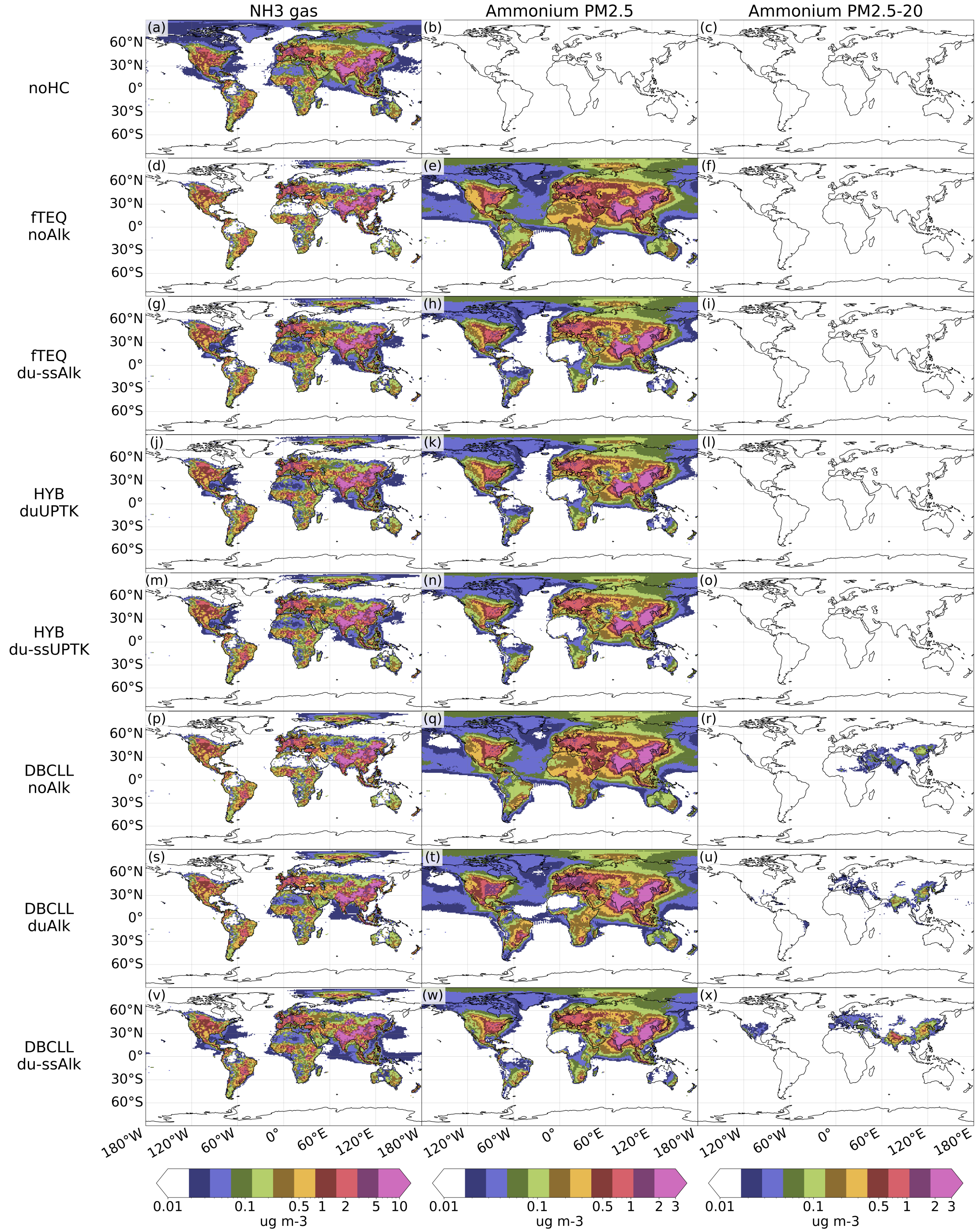

Figure S4. Surface concentrations ($\mu g\ m^{-3}$) of $NH_{3(g)}$, fine and coarse particulate ammonium simulated by the different mechanisms, averaged for 2018.

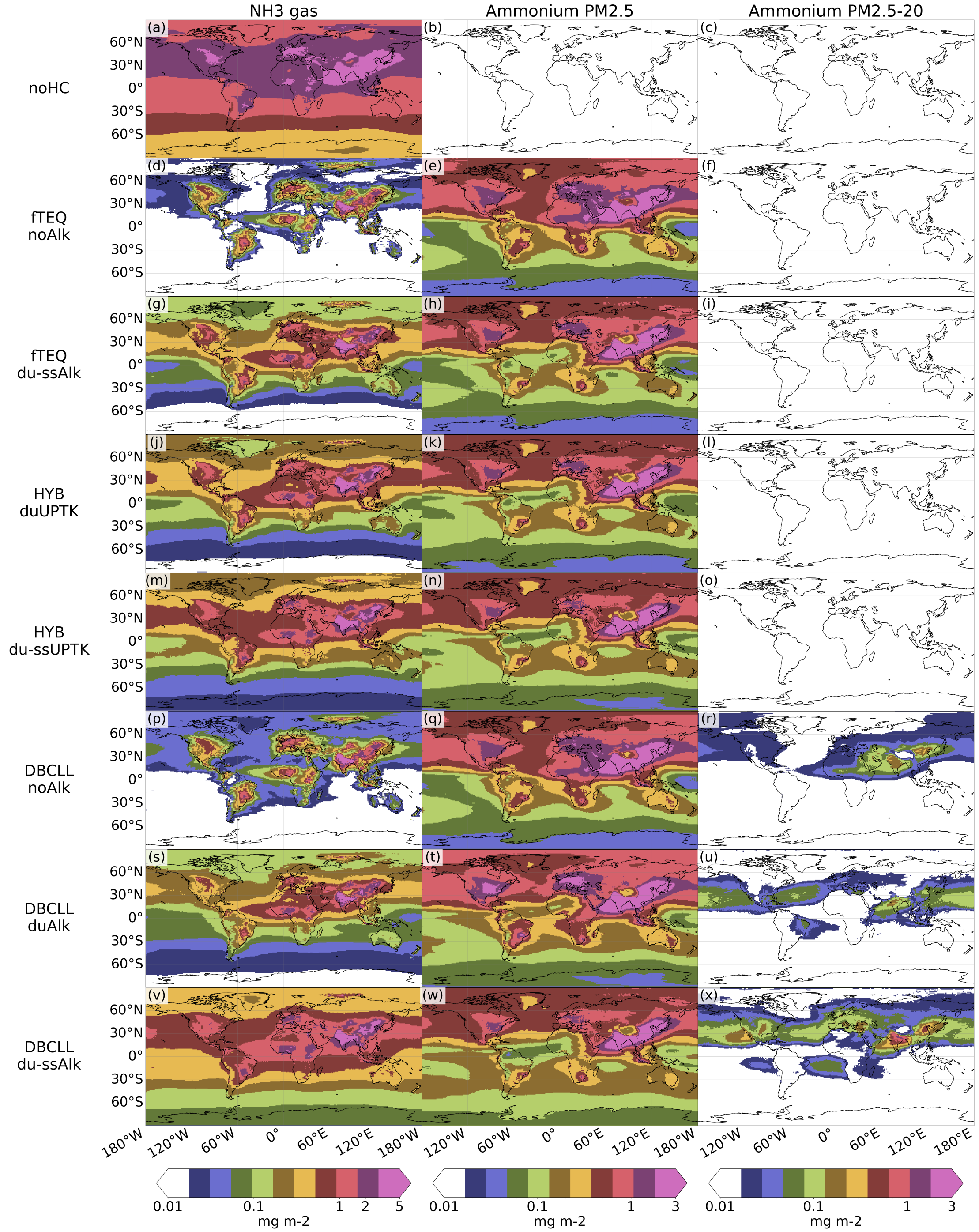

Figure S5. Column loads ($mg\ m^{-2}$) of $NH_{3(g)}$, fine and coarse particulate ammonium simulated by different mechanisms, averaged for 2018.

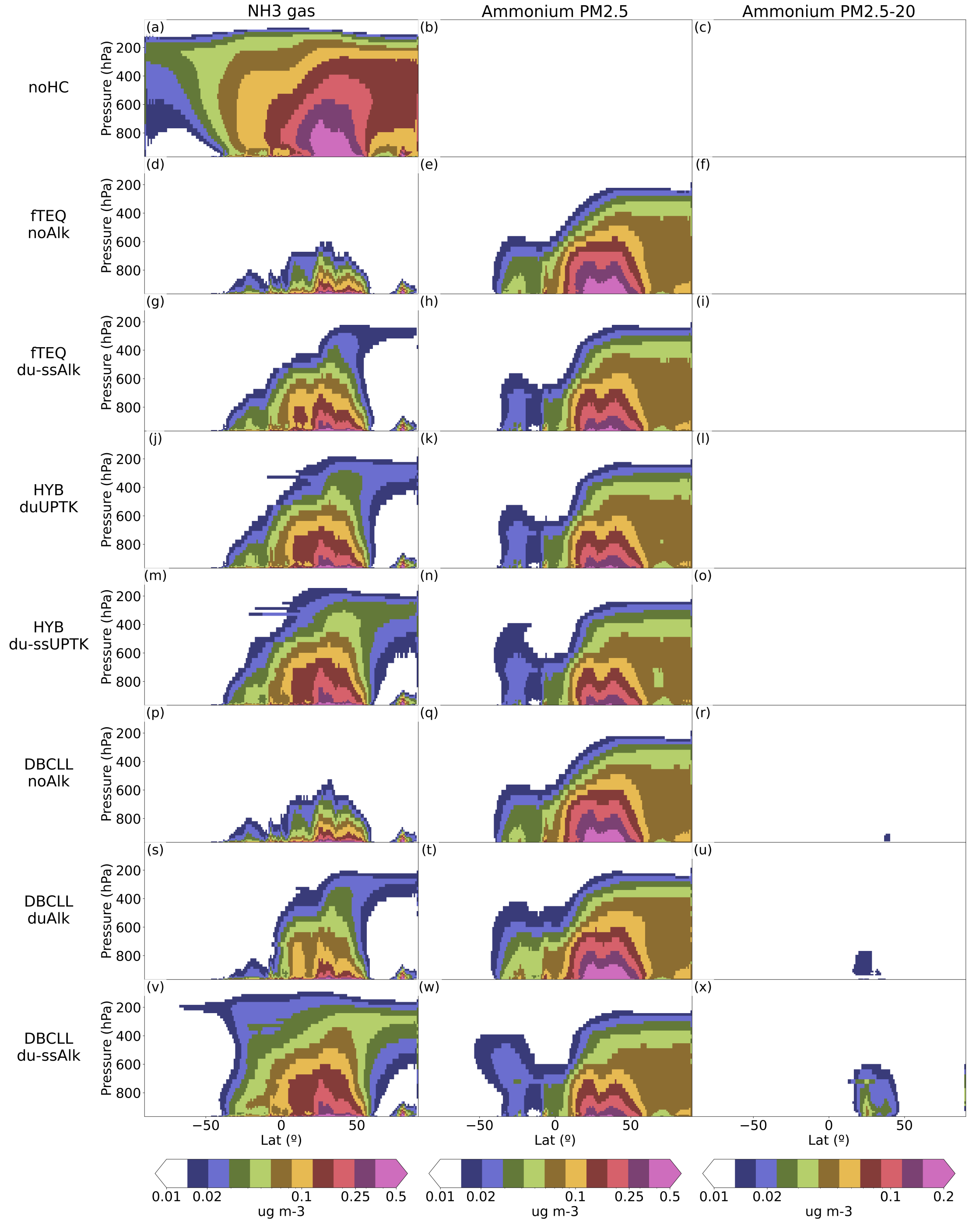

Figure S6. Zonal average concentrations ($\mu g\, m^{-3}$) of $NH_{3(g)}$, fine and coarse particulate ammonium simulated by the different mechanisms, averaged for 2018.

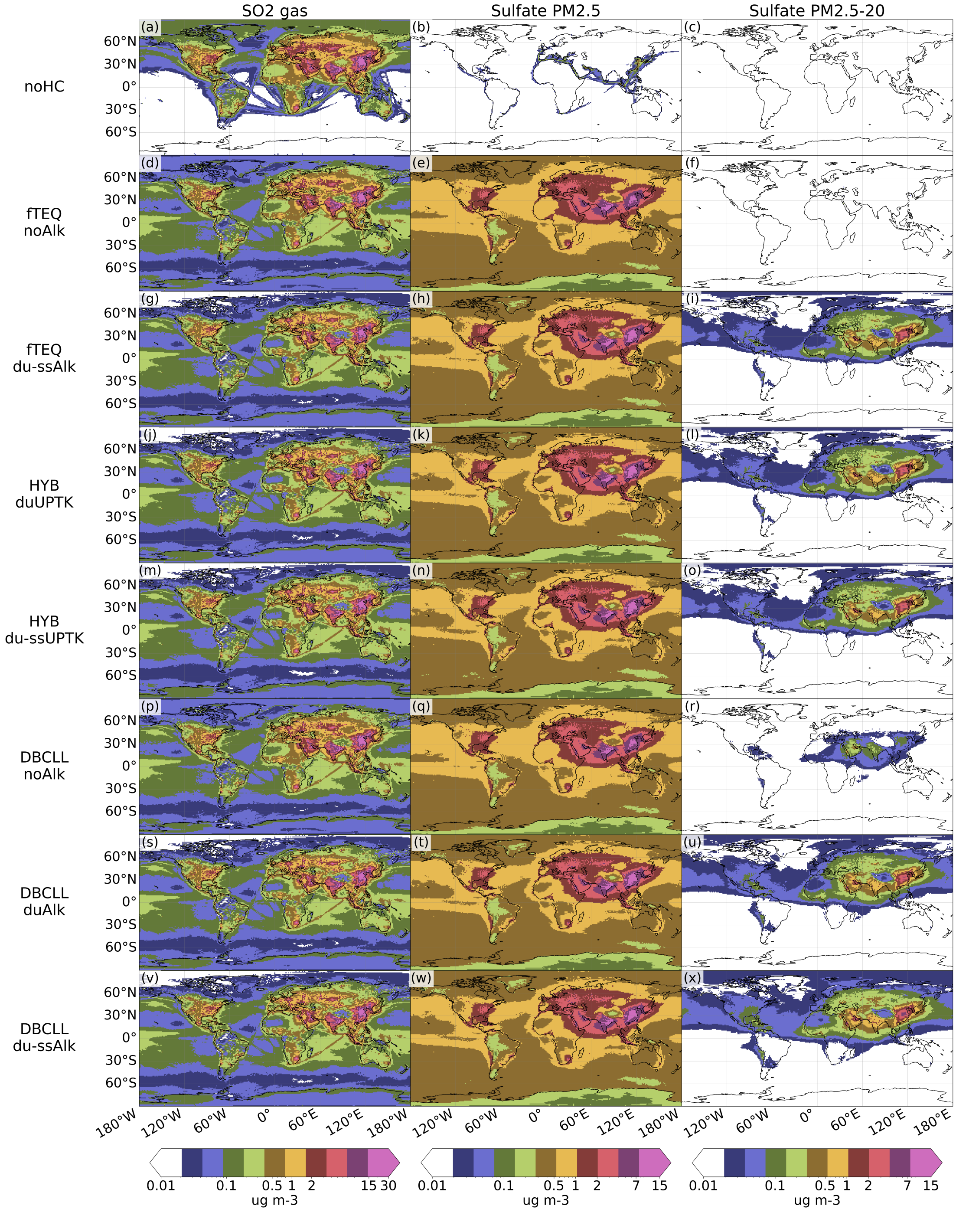

Figure S7. Surface concentration ($\mu g\ m^{-3}$) of $SO_{2(g)}$, fine and coarse particulate sulfate SO_4^{2-} simulated by the different mechanisms, averaged for 2018.

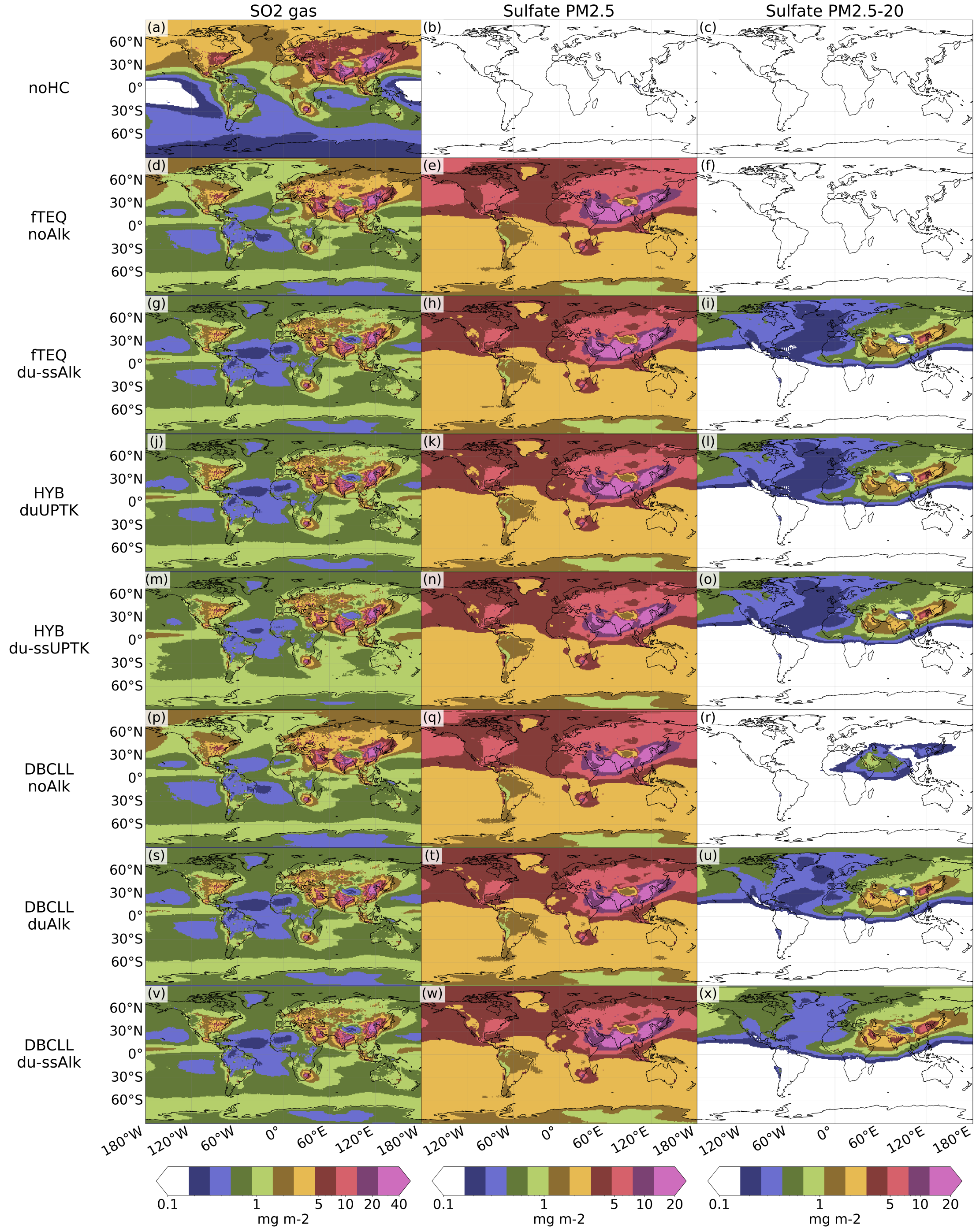

Figure S8. Column load ($mg\ m^{-2}$) of $SO_{2(g)}$, fine and coarse particulate sulfate SO_4^{2-} simulated by the different mechanisms, averaged for 2018.

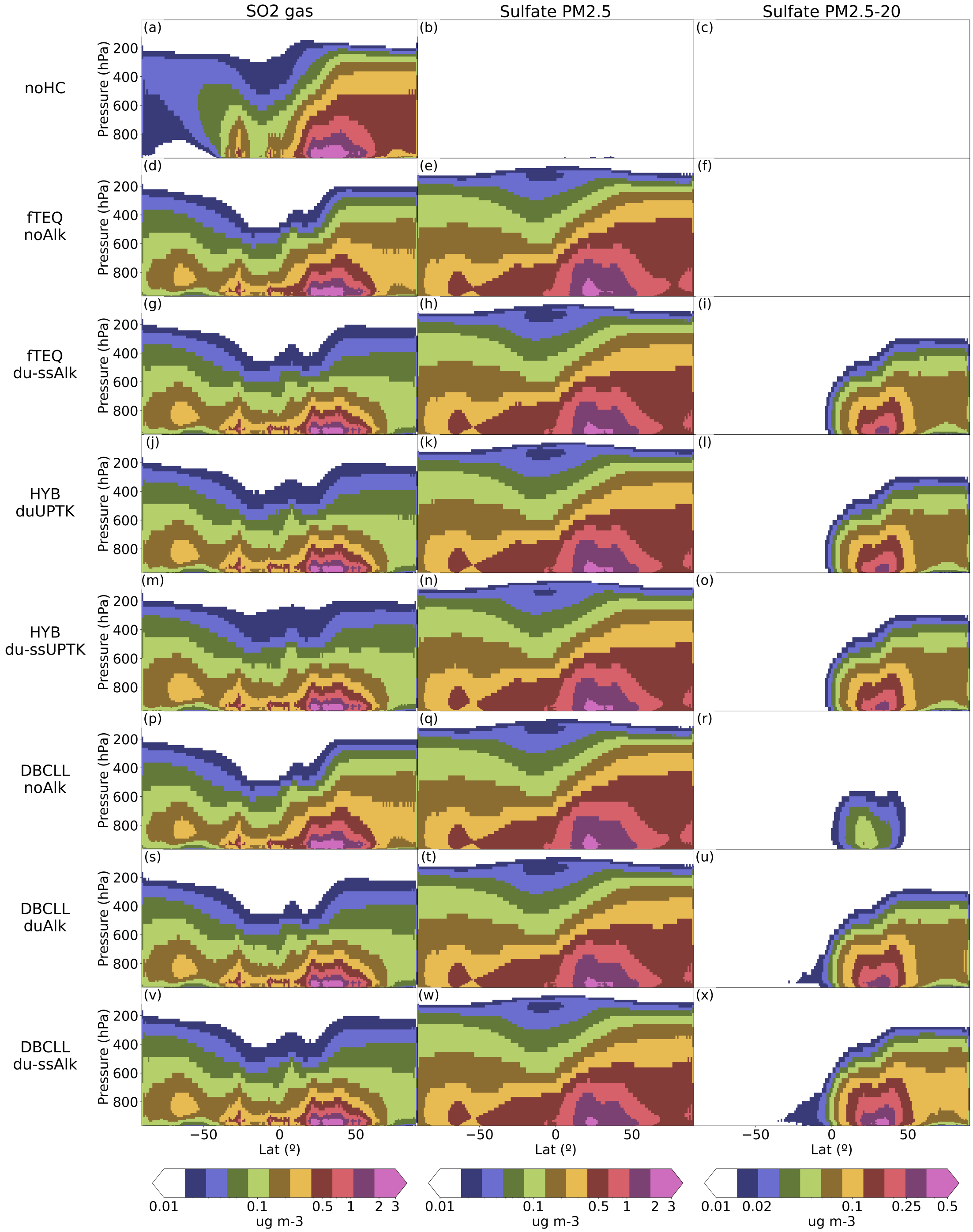

Figure S9. Zonal average concentration ($\mu g\ m^{-3}$) of $SO_{2(g)}$, fine and coarse particulate sulfate SO_4^{2-} simulated by the different mechanisms, averaged for 2018.

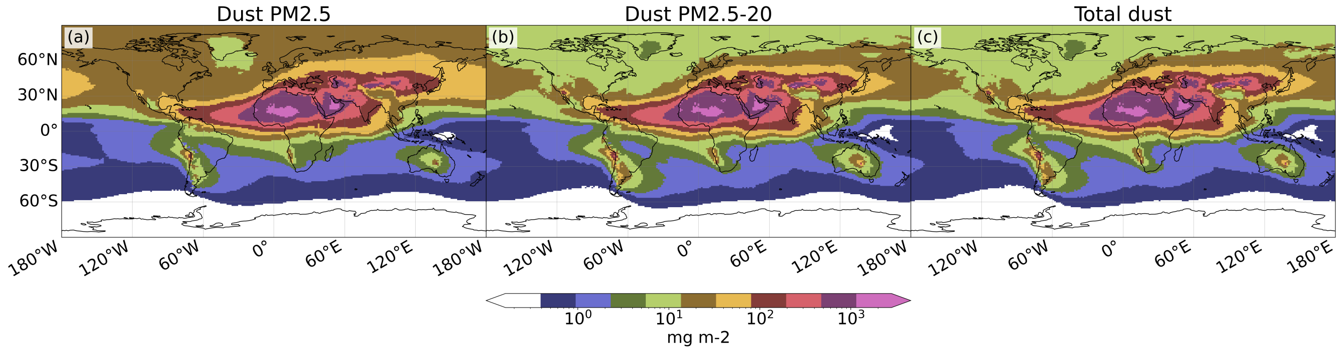

Figure S10. Dust average column load (mgm^{-2}) for 2018.

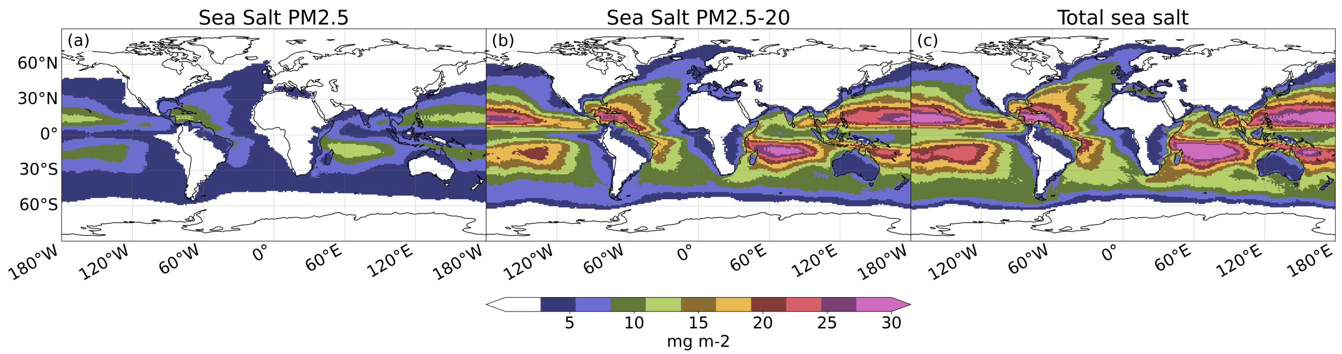

Figure S11. Sea salt average column load (mgm^{-2}) for 2018.

S3 Statistical metrics and supplementary evaluation results

Each experiment is evaluated against observations in terms of correlation coefficient (corr), mean bias (bias) and root mean square error (rmse), formulated as follows:

$$corr = \frac{\sum_{i=1}^{N}(S_i - \bar{S})(O_i - \bar{O})}{\sqrt{\sum_{i=1}^{N}(S_i - \bar{S})^2}\sqrt{\sum_{i=1}^{N}(O_i - \bar{O})^2}} \tag{1}$$

$$bias = \frac{\sum_{i=1}^{N}(S_i - O_i)}{N} \tag{2}$$

$$rmse = \sqrt{\frac{\sum_{i=1}^{N}(S_i - O_i)^2}{N}} \tag{3}$$

Where *S* are the simulation results, *O* the observations and *N* the number of observations.

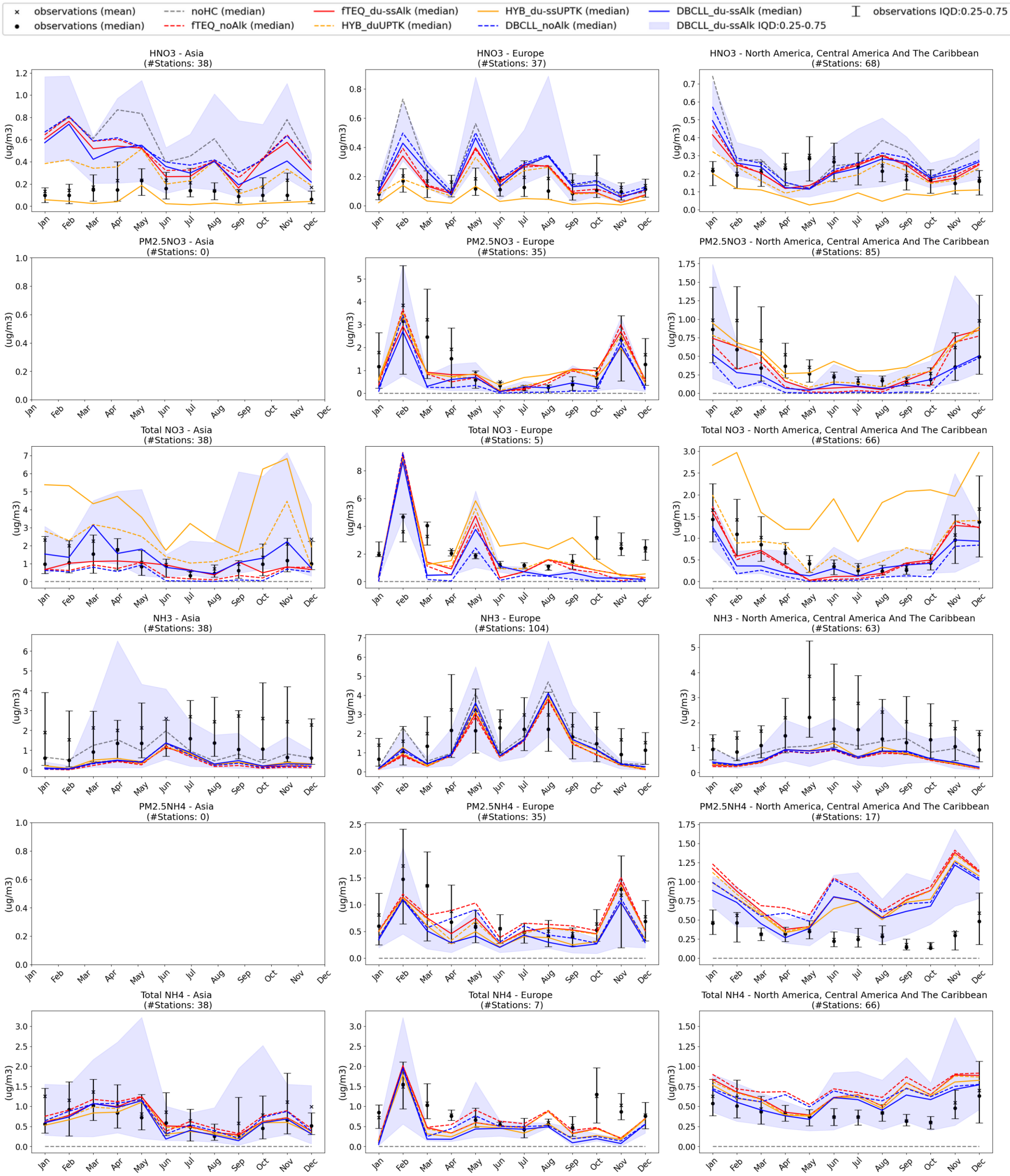

Figure S12. Yearly surface concentration evaluation for Asia, Europe and North-Central America continents. Species are in rows and continents in columns. Black solid dots and crosses represent observational mean and median, respectively. Error bars are the interquantile 0.25 to 0.75 distance. Coloured lines represent medians obtained from the most representative configurations. Blue shade is the interquantile 0.25 - 0.75 distance for the DBCLL_du-ssAlk simulation. Observational PM_{10} from EANET (Asia) and US-EPA-CASTNET (North America) refers to total particle concentration, while GHOST data (Europe) is limited to PM_{10}. (Continues in the next page)

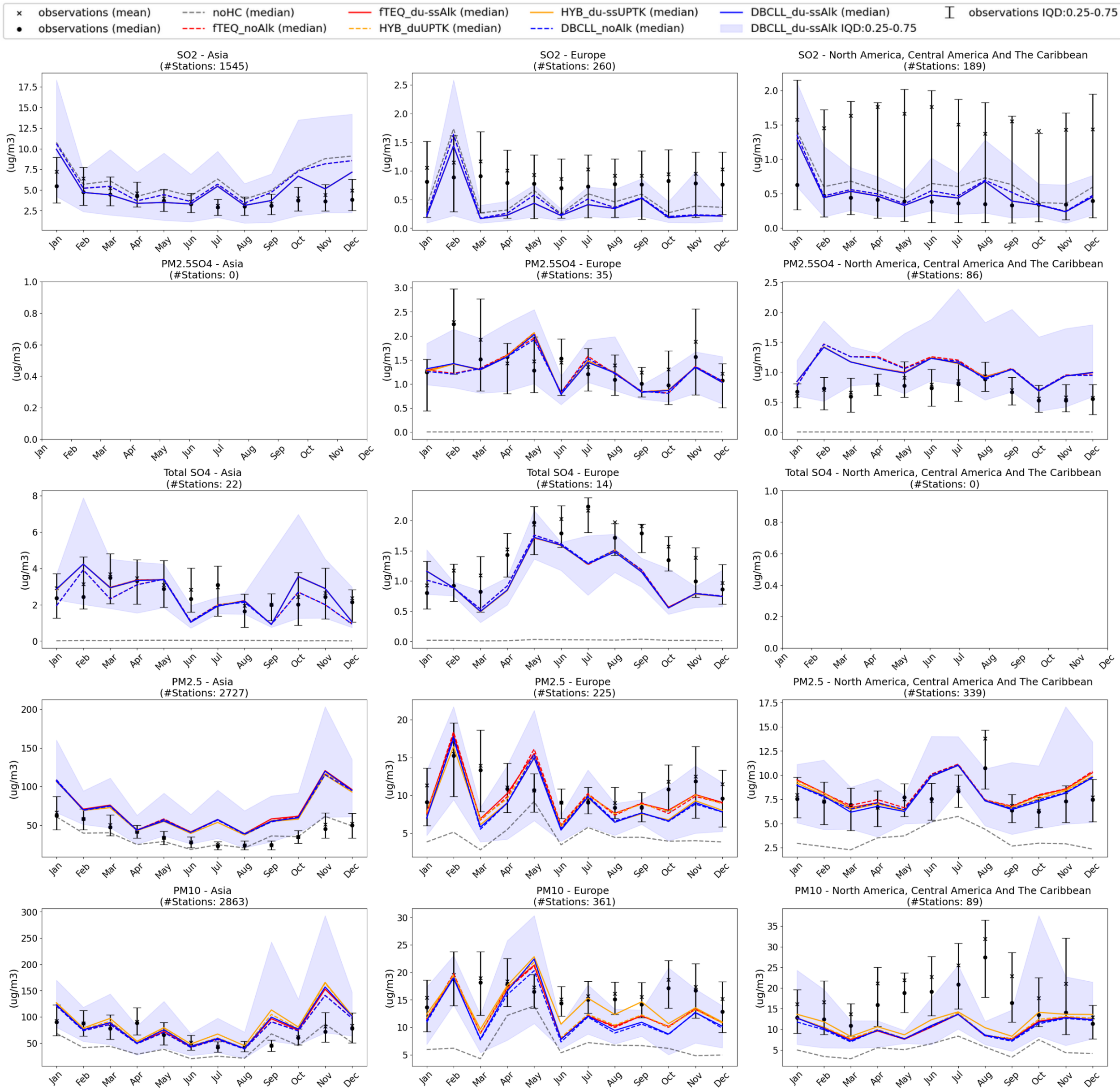

Figure S12. (Continuation) Yearly surface concentration evaluation for Asia, Europe and North-Central America continents. Species are in rows and continents in columns. Black solid dots and crosses represent observational mean and median, respectively. Error bars are the interquantile 0.25 to 0.75 distance. Coloured lines represent medians obtained from the most representative configurations. Blue shade is the interquantile 0.25 - 0.75 distance for the DBCLL_du-ssAlk simulation. Observational PM_{10} from EANET (Asia) and US-EPA-CASTNET (North America) for sulfate refers to total particle concentration, while GHOST data (Europe) is limited to PM_{10}.

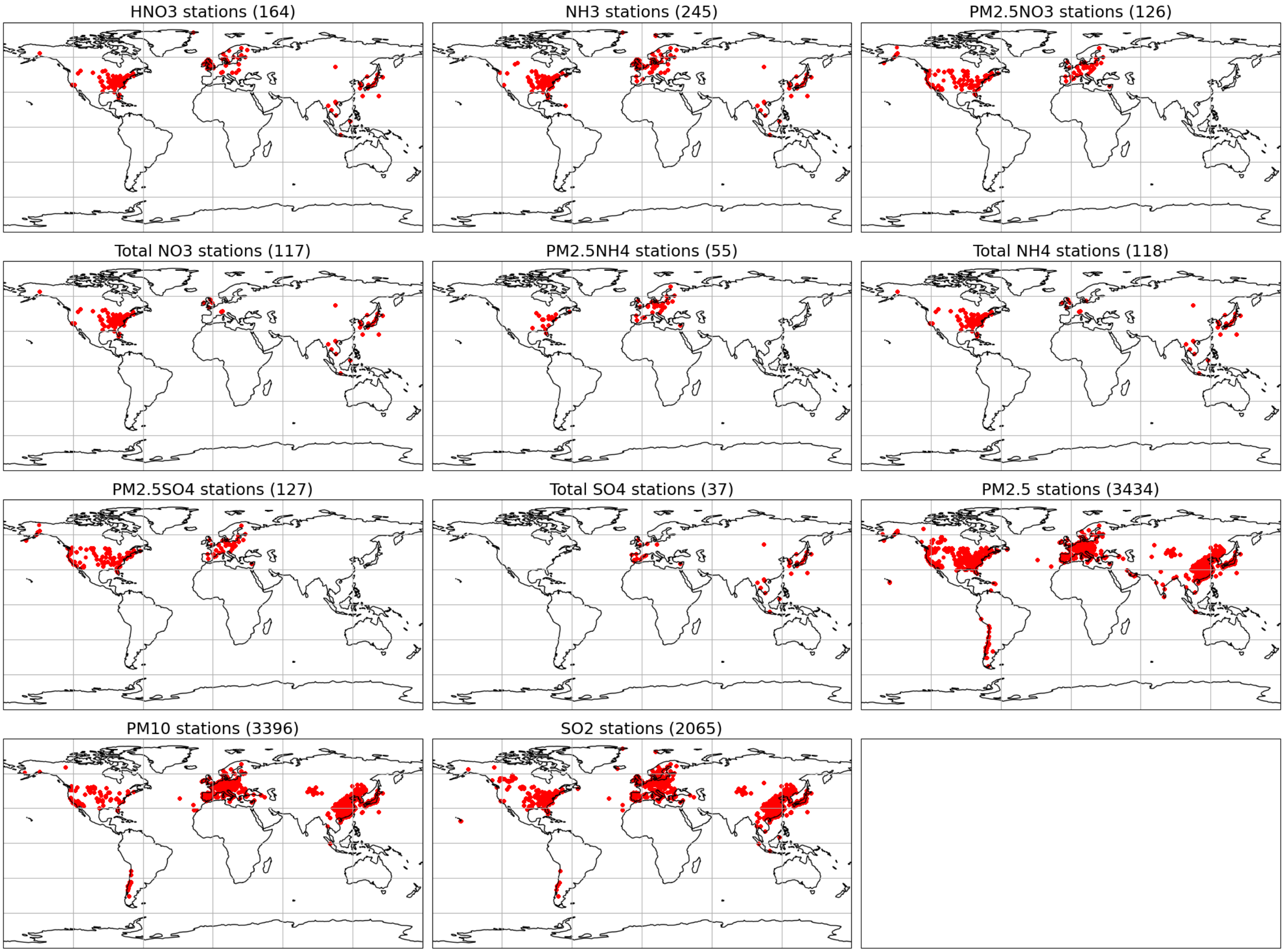

Figure S13. Stations used in the observational evaluation for each species from the main text Fig. 5 and Supplement Fig. S12.

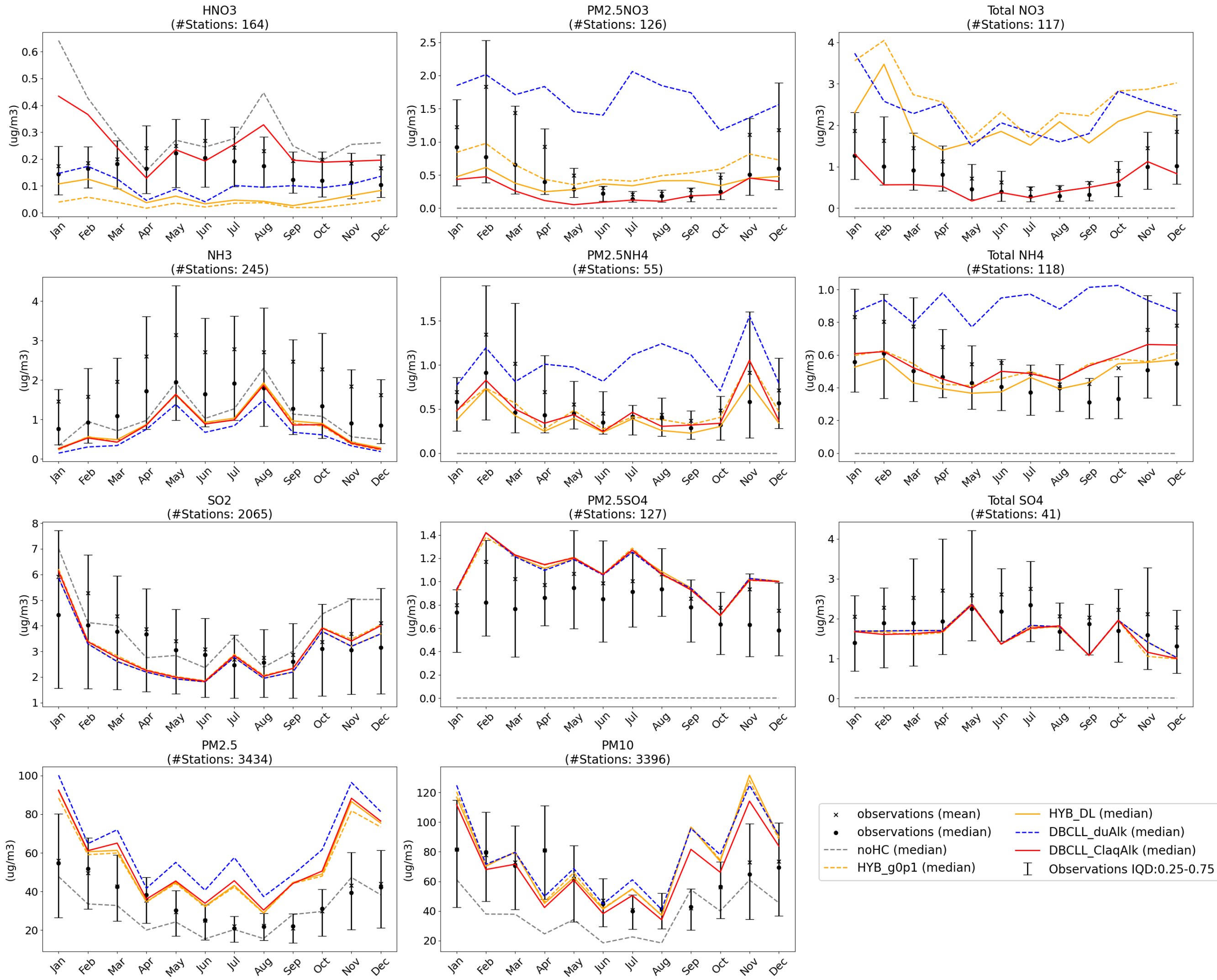

Figure S14. Observational evaluation of gas and particulate species of additional sensitivity experiments. Black solid dots and crosses represent monthly mean and median of observations, respectively. Colour lines represent each configuration's monthly median surface concentrations over observational points. Error bars are the observational interquantile 0.25 to 0.75 distance. For the Total NO_3 modes, data from Europe, Asia and North-Central America has been averaged, despite data from Asia and North-Central America refers to total particle concentration, while data from Europe is limited strictly to $10\mu m$ particle diameter.

Table S7: Correlation coefficients, bias ($\mu g\ m^{-3}$) and root mean square error (rmse, $\mu g\ m^{-3}$) of additional sensitivity experiments. The evaluation corresponds to the configurations' median with respect to the median of observations, corresponding to the timeseries shown in Fig. S14.

	HNO3			**PM2.5NO3**			**Total NO3**		
	corr	**bias**	**rmse**	**corr**	**bias**	**rmse**	**corr**	**bias**	**rmse**
noHC	0.03	0.15	0.20	0.00	-0.43	0.49	0.00	-0.70	0.77
HYB_g0p1	0.05	-0.13	0.13	0.83	0.18	0.23	0.81	1.96	2.01
HYB_DL	-0.08	-0.10	0.11	0.61	-0.03	0.21	0.53	1.32	1.40
DBCLL_duAlk	-0.34	-0.05	0.08	0.21	1.24	1.28	0.80	1.61	1.65
DBCLL_ClaqAlk	0.14	0.09	0.12	0.82	-0.18	0.24	0.81	-0.09	0.22

	NH3			**PM2.5NH4**			**Total NH4**		
	corr	**bias**	**rmse**	**corr**	**bias**	**rmse**	**corr**	**bias**	**rmse**
noHC	0.80	-0.29	0.44	0.00	-0.48	0.51	0.00	-0.45	0.46
HYB_g0p1	0.85	-0.53	0.59	0.64	0.01	0.16	0.47	0.07	0.11
HYB_DL	0.85	-0.49	0.56	0.77	-0.09	0.14	0.50	0.02	0.09
DBCLL_duAlk	0.88	-0.71	0.73	0.27	0.53	0.58	-0.46	0.46	0.48
DBCLL_ClaqAlk	0.85	-0.53	0.59	0.70	-0.01	0.16	0.50	0.09	0.12

	SO2			**PM2.5SO4**			**Total SO4**		
	corr	**bias**	**rmse**	**corr**	**bias**	**rmse**	**corr**	**bias**	**rmse**
noHC	0.61	0.65	1.24	0.59	-0.79	0.80	0.62	-1.91	1.93
HYB_g0p1	0.62	-0.12	0.94	0.59	0.29	0.32	0.53	-0.42	0.54
HYB_DL	0.63	-0.29	0.91	0.57	0.29	0.33	0.60	-0.39	0.50
DBCLL_duAlk	0.63	-0.29	0.91	0.55	0.29	0.32	0.59	-0.38	0.49
DBCLL_ClaqAlk	0.62	-0.16	0.94	0.57	0.29	0.33	0.55	-0.41	0.52

	PM2.5			**PM10**		
	corr	**bias**	**rmse**	**corr**	**bias**	**rmse**
noHC	0.75	-5.62	9.55	0.40	-23.16	28.42
HYB_g0p1	0.76	18.02	21.95	0.38	14.27	29.96
HYB_DL	0.76	19.44	23.81	0.36	13.87	30.41
DBCLL_duAlk	0.71	28.07	31.58	0.38	16.47	30.10

Table S7 continued from previous page

DBCLL_ClaqAlk	0.76	20.75	24.88	0.43	7.45	24.20

Table S8. GHOST quality flags used for the observational evaluation.

Code	Flag	Description
0	Missing Measurement	i.e. NaN.
1	Infinite Value	Value is infinite – occurs when data values are outside of the range that *float32* data type can handle (-3.4E+38 to +3.4E+38).
2	Negative Measurement	Measurement is negative in absolute terms.
6	Invalid Data Provider Flags - GHOST Decreed	Measurements are associated with data quality flags given by the data provider which have been decreed by the GHOST project architects as being associated with substantial uncertainty/bias.
8	No Valid Data to Average	After screening by key QA flags, no valid data remains to average in the temporal window.
20	Erroneous Primary Sampling	The primary sampling is not appropriate to prepare the specific parameter for subsequent measurement.
21	Erroneous Sample Preparation	The sample preparation is not appropriate to prepare the specific parameter for subsequent measurement.
22	Erroneous Measurement Methodology	The measurement methodology used is not known to be able to measure the specific parameter.
72	Below Preferential Lower Limit of Detection	Measurement is below or equal to the preferential lower limit of detection.
75	Above Preferential Upper Limit of Detection	Measurement is above or equal to the preferential upper limit of detection.
82	Insufficient Measurement Resolution - Preferential	The preferential resolution for the measurement is coarser than a set limit (variable by measured parameter).
83	Insufficient Measurement Resolution - Empirical	The resolution of the measurement is analysed month by month. If the minimum difference between observations is coarser than a set limit (variable by measured parameter), measurements are flagged.
110	Data Outlier - Exceeds Scientifically Decreed Lower/Upper Limit	The measured value is below or greater than scientifically feasible lower/upper limits (variable by parameter).
111	Data Outlier - Monthly Median Exceeds Scientifically Decreed Upper Limit	The median of the measurements in a month is greater than a scientifically feasible limit (variable by parameter).
112	Data Outlier - Network Decreed	Data has been reported to be an outlier through data flags by the network data reporters (and not manually checked and verified as valid).
113	Data Outlier - Manually Decreed	Data has been found and decreed manually to be an outlier.
115	Probable Data Outlier - Monthly Adjusted Boxplot	Measured value exceeds adjusted boxplot outer fence (lower or upper) of monthly data, therefore is a probable data outlier.
132	Systematic Inconsistent Monthly Distributions - 4/6 Months >= Zone 6	4 out of 6 months' distributions are classed as Zone 6 or higher, suggesting there are potentially systematic reasons for the inconsistent distributions across the 6 months.
133	Systematic Inconsistent Monthly Distributions - 8/12 Months >= Zone 6	8 out of 12 months' distributions are classed as Zone 6 or higher, suggesting there are potentially systematic reasons for the inconsistent distributions across the 12 months.

S4 Budget tables

Table S9. Results for gas $HNO_{3(g)}$ obtained with the studied heterogeneous chemistry mechanisms. Results from the literature references are reported at the end of the table: The average of all the participating models in the intercomparison AeroCom phase III nitrate experiment for 2008 (*AeroCom*), specifying their standard deviation (*STD AeroCom*), results from the GMI model (*GMI*, using a similar HYB approach with UPTK reactions on dust and SS), and results from the EMAC model (*EMAC 2008*, using a similar approach to DBCLL_du-ssAlk). Also using the EMAC model, results obtained by the Karydis et al. (2016) study are reported as *EMAC 2005-2008*. Results from models using a similar approach to HYB_du-ssUPTK are reported as *IFS* for Rémy et al. (2022), *LMDz-INCA* for Hauglustaine et al. (2014) and *MetOffice UM* for Jones et al. (2021).

$HNO_{3(g)}$	**Burden (Tg)**	**Wet Dep. (Tg y-1)**	**Dry Dep. (Tg y-1)**	**Total Dep. (Tg y-1)**	**Production (Tg y-1)**	**Lifetime (days)**
noHC	4.79	47.1	110.4	157.5	158.3	5.5
fTEQ_noAlk	4.99	48.6	107.3	155.9	156.7	5.8
fTEQ_du-ssAlk	2.93	41.4	77.4	118.8	119.3	4.5
HYB_duUPTK	1.96	29.9	52.0	81.9	82.4	4.4
HYB_du-ssUPTK	0.69	7.2	13.7	20.9	21.4	5.9
HYB_gDU=0.1	0.46	5.9	5.9	11.8	12.2	7.1
HYB_DL	0.72	6.7	14.0	20.7	21.2	6.2
DBCLL_noAlk	5.13	49.1	109.1	158.2	159.0	5.9
DBCLL_duAlk	2.72	45.4	59.9	105.3	105.7	4.7
DBCLL_du-ssAlk	2.53	36.1	61.9	98.0	98.6	4.7
DBCLL_ClaqAlk	2.58	36.2	62.1	98.3	98.9	4.8
AeroCom	**2.50**	**108.7**	**45.8**	**154.5**	**179.0**	**4.6**
STD AeroCom	**±1.83**	**±39.8**	**±13.0**	**±52.8**	**±89.9**	**±1.6**
GMI	**2.50**	**108.7**	**45.8**	**154.5**	**110.0**	**3.5**
EMAC 2008[1]	**3.10**	**136.0**	**56.1**	**192.1**	**-**	**-**
EMAC 2005-2008[2]	**1.65**	**-**	**-**	**-**	**-**	**-**
IFS	**-**	**-**	**-**	**-**	**-**	**-**
LMDz-INCA	**1.35**	**76.6**	**66.0**	**142.6**	**218.3**	**2.3**
MetOffice UM[3]	**2.16**	**67.1**	**27.0**	**94.1**	**242.1**	**3.2**

[1] From Bian et al. (2017).

[2] From Karydis et al. (2016).

[3] Jones et al. (2021) performs two sensitivity tests to the accommodation coefficient used for NO_3^- formation in the fine mode: *FAST* with 0.193 and *SLOW* with 0.001. Here, results from the *FAST* test are reported on the basis that they present similar fine NO_3^- formation rates to our average fine nitrate results

Table S10. Results for gas $NH_{3(g)}$ obtained with the studied heterogeneous chemistry mechanisms. Results from the literature references are reported at the end of the table: The average of all the participating models in the intercomparison AeroCom phase III nitrate experiment for 2008 (*AeroCom*), specifying their standard deviation (*STD AeroCom*), results from the GMI model (*GMI*, using a similar HYB approach with UPTK reactions on dust and SS), and results from the EMAC model (*EMAC 2008*, using a similar approach to DBCLL_du-ssAlk). Also using the EMAC model, results obtained by the Karydis et al. (2016) study are reported as *EMAC 2005-2008*. Results from models using a similar approach to HYB_du-ssUPTK are reported as *IFS* for Rémy et al. (2022), *LMDz-INCA* for Hauglustaine et al. (2014) and *MetOffice UM* for Jones et al. (2021).

$NH_{3(g)}$	**Emissions (Tg y-1)**	**Burden (Tg)**	**Wet Dep. (Tg y-1)**	**Dry Dep. (Tg y-1)**	**Total Dep. (Tg y-1)**	**Loss (Tg y-1)**	**Lifetime (days)**
noHC	61.8	0.86	7.1	54.5	61.7	0.0	5.1
fTEQ_noAlk	61.8	0.05	1.3	39.6	40.9	-20.9	0.3
fTEQ_du-ssAlk	61.8	0.16	1.8	44.2	45.9	-15.9	0.9
HYB_duUPTK	61.8	0.21	1.9	44.7	46.6	-15.1	1.2
HYB_du-ssUPTK	61.8	0.26	2.2	45.6	47.8	-14.0	1.5
HYB_gDU=0.1	61.8	0.28	2.2	46.0	48.3	-13.5	1.7
HYB_DL	61.8	0.38	2.9	46.7	49.6	-12.1	2.2
DBCLL_noAlk	61.8	0.06	1.6	40.4	42.0	-19.8	0.4
DBCLL_duAlk	61.8	0.14	1.8	39.8	41.7	-20.2	0.8
DBCLL_du-ssAlk	61.8	0.35	2.8	45.9	48.6	-13.2	2.0
DBCLL_ClaqAlk	61.8	0.31	2.7	45.5	48.2	-13.6	1.8
AeroCom	**62.9**	**0.20**	**13.4**	**18.7**	**32.1**	**-32.1**	**0.7**
STD AeroCom	**±3.9**	**±0.20**	**±5.1**	**±5.1**	**±10.2**	**±12.0**	**±0.3**
GMI	**60.4**	**0.85**	**1.1**	**8.7**	**9.8**	**-50.1**	**5.2**
EMAC 2008[1]	**59.3**	**0.85**	**0.0**	**15.5**	**15.5**	**-**	**-**
EMAC 2005-2008[2]	**-**	**0.82**	**-**	**-**	**-**	**-**	**-**
IFS	**-**	**-**	**-**	**-**	**-**	**-**	**-**
LMDz-INCA	**61.3**	**0.11**	**13.4**	**25.9**	**39.3**	**-21.2**	**0.6**
MetOffice UM[3]	**64.7**	**0.05**	**6.9**	**21.1**	**28.0**	**-36.8**	**0.3**

[1] From Bian et al. (2017).

[2] From Karydis et al. (2016).

[3] Jones et al. (2021) performs two sensitivity tests to the accommodation coefficient used for NO_3^- formation in the fine mode: *FAST* with 0.193 and *SLOW* with 0.001. Here, results from the *FAST* test are reported on the basis that they present similar fine NO_3^- formation rates to our average fine nitrate results.

Table S11. Results fine, coarse and total particulate NH_4^+ obtained with the studied heterogeneous chemistry mechanisms. Results from the literature references are reported at the end of the table: The average of all the participating models in the intercomparison AeroCom phase III nitrate experiment for 2008 (*AeroCom*), specifying their standard deviation (*STD AeroCom*), results from the GMI model (*GMI*, using a similar HYB approach with UPTK reactions on dust and SS), and results from the EMAC model (*EMAC 2008*, using a similar approach to DBCLL_du-ssAlk). Also using the EMAC model, results obtained by the Karydis et al. (2016) study are reported as *EMAC 2005-2008*. Results from models using a similar approach to HYB_du-ssUPTK are reported as *IFS* for Rémy et al. (2022), *LMDz-INCA* for Hauglustaine et al. (2014) and *MetOffice UM* for Jones et al. (2021).

NH_4^+	**Burden (Tg)**			**Wet Dep. (Tg y-1)**			**Dry Dep. (Tg y-1)**			**Total Dep. (Tg y-1)**			**Production (Tg y-1)**			**Lifetime (days)**		
Experiment	Fine	Coarse	**Total**	Fine	Coarse	**Total**	Fine	Coarse	**Total**	Fine	Coarse	**Total**	Fine	Coarse	**Total**	Fine	Coarse	**Total**
fTEQ_noAlk	0.30	0.00	**0.30**	19.2	0.0	**19.2**	3.0	0.0	**3.0**	22.2	0.0	**22.2**	22.2	0.0	**22.2**	2.5	0.0	**2.5**
fTEQ_du-ssAlk	0.21	0.00	**0.21**	14.9	0.0	**14.9**	2.0	0.0	**2.0**	16.9	0.0	**16.9**	16.9	0.0	**16.9**	2.3	0.0	**2.3**
HYB_duUPTK	0.21	0.00	**0.21**	14.3	0.0	**14.3**	1.9	0.0	**1.9**	16.2	0.0	**16.2**	16.2	0.0	**16.2**	2.3	0.0	**2.3**
HYB_du-ssUPTK	0.20	0.00	**0.20**	13.2	0.0	**13.2**	1.7	0.0	**1.7**	15.0	0.0	**15.0**	15.0	0.0	**15.0**	2.4	0.0	**2.4**
HYB_gDU=0.1	0.19	0.00	**0.19**	12.9	0.0	**12.9**	1.6	0.0	**1.6**	14.5	0.0	**14.5**	14.5	0.0	**14.5**	2.4	0.0	**2.4**
HYB_DL	0.19	0.00	**0.19**	11.7	0.0	**11.7**	1.6	0.0	**1.6**	13.3	0.0	**13.3**	13.3	0.0	**13.3**	2.7	0.0	**2.7**
DBCLL_noAlk	0.29	0.01	**0.30**	17.8	0.3	**18.1**	2.8	0.2	**2.9**	20.5	0.5	**21.0**	20.5	0.5	**21.0**	2.6	3.1	**2.6**
DBCLL_duAlk	0.30	0.01	**0.31**	18.9	0.3	**19.2**	3.1	0.2	**3.3**	22.1	0.4	**22.5**	22.1	0.4	**22.5**	2.5	4.1	**2.5**
DBCLL_du-ssAlk	0.20	0.02	**0.22**	12.6	0.2	**12.7**	1.8	0.1	**1.9**	14.3	0.3	**14.6**	14.3	0.3	**14.6**	2.6	10.8	**2.8**
DBCLL_ClaqAlk	0.22	0.02	**0.23**	12.9	0.2	**13.1**	1.8	0.2	**2.0**	14.7	0.4	**15.1**	14.7	0.4	**15.1**	2.7	7.7	**2.8**
AeroCom	-	-	**0.32**	-	-	**24.4**	-	-	**5.8**	-	-	**30.2**	-	-	**30.4**	-	-	**4.3**
STD AeroCom	-	-	**±0.20**	-	-	**±10.0**	-	-	**±5.8**	-	-	**±15.8**	-	-	**±4.3**	-	-	**±2.6**
GMI	-	-	**0.48**	-	-	**50.7**	-	-	**1.9**	-	-	**52.6**	-	-	**53.0**	-	-	**3.4**
EMAC 2008[1]	-	-	**0.19**	-	-	**44.5**	-	-	**3.6**	-	-	**48.1**	-	-	**-**	-	-	**-**
EMAC 2005-2008[2]	-	-	**0.17**	-	-	**-**	-	-	**-**	-	-	**-**	-	-	**-**	-	-	**-**
IFS[3]	-	-	**0.15**	-	-	**17.4**	-	-	**1.4**	-	-	**18.8**	-	-	**18.6**	-	-	**2.9**
LMDz-INCA	-	-	**0.28**	-	-	**19.2**	-	-	**3.2**	-	-	**22.4**	-	-	**22.4**	-	-	**4.5**
MetOffice UM[4]	-	-	**0.54**	-	-	**32.1**	-	-	**7.4**	-	-	**32.1**	-	-	**39.2**	-	-	**5.0**

1. From Bian et al. (2017).
2. From Karydis et al. (2016).
3. Fine NO_3^- reported from neutralization of nitric acid, ammonia and sulfate. Coarse nitrate from heterogeneous chemistry (Rémy et al., 2022).
4. Jones et al. (2021) performs two sensitivity tests to the accommodation coefficient used for NO_3^- formation in the fine mode: *FAST* with 0.193 and *SLOW* with 0.001. Here, results from the *FAST* test are reported on the basis that they present similar fine NO_3^- formation rates to our average fine nitrate results

Table S12. Results for $SO_{2(g)}$, and fine, coarse and total particulate SO_4^{2-} obtained with the studied heterogeneous chemistry mechanisms. Results from the literature references are reported at the end of the table: The average of all the participating models in the intercomparison AeroCom phase III nitrate experiment for 2008 (*AeroCom*), specifying their standard deviation (*STD AeroCom*), results from the GMI model (*GMI*, using a similar HYB approach with UPTK reactions on dust and SS), and results from the EMAC model (*EMAC 2008*, using a similar approach to DBCLL_du-ssAlk). Also using the EMAC model, results obtained by the Karydis et al. (2016) study are reported as *EMAC 2005-2008*. Results from models using a similar approach to HYB_du-ssUPTK are reported as *IFS* for Rémy et al. (2022), *LMDz-INCA* for Hauglustaine et al. (2014) and *MetOffice UM* for Jones et al. (2021).

SO_4^{2-}	SO4 Emissions (Tg y-1)		SO2 Emissions (Tg y-1)	SO4 Burden (Tg)			SO4 Wet Dep. (Tg y-1)			SO4 Dry Dep. (Tg y-1)			SO4 Total Dep. (Tg y-1)			SO4 Production (Tg y-1)			SO4 Lifetime (days)		
Experiment	Fine	Coarse	**Total**	Fine	Coarse	**Total**	Fine	Coarse	**Total**	Fine	Coarse	**Total**	Fine	Coarse	**Total**	Fine	Coarse	**Total**	Fine	Coarse	**Total**
noHC	0.5	0.0	**104.4**	4.4E-3	0.00	**0.00**	0.5	0.0	**0.5**	0.1	0.0	**0.1**	0.5	0.0	**0.5**	0.0	0.0	**0.0**	3.1	0.0	**3.0**
fTEQ_noAlk	0.5	0.0	**104.4**	1.98	0.00	**1.98**	126.9	0.0	**126.9**	13.5	0.0	**13.5**	140.5	0.0	**140.5**	139.9	0.0	**139.9**	2.6	0.9	**2.6**
fTEQ_du-ssAlk	0.5	0.0	**104.4**	1.82	0.14	**1.96**	116.7	6.9	**123.6**	13.0	3.5	**16.5**	129.7	10.4	**140.1**	129.1	10.4	**139.5**	2.6	2.4	**2.6**
HYB_duUPTK	0.5	0.0	**104.4**	1.82	0.14	**1.96**	116.5	7.0	**123.5**	13.0	3.5	**16.4**	129.4	10.5	**139.9**	128.9	10.5	**139.3**	2.6	2.4	**2.6**
HYB_du-ssUPTK	0.5	0.0	**104.4**	1.85	0.14	**1.98**	116.4	7.1	**123.5**	12.9	3.5	**16.4**	129.3	10.6	**139.9**	128.7	10.6	**139.3**	2.6	2.4	**2.6**
HYB_gDU=0.1	0.5	0.0	**104.4**	1.87	0.12	**1.99**	117.8	6.1	**124.0**	12.7	2.9	**15.7**	130.6	9.1	**139.7**	130.0	9.0	**139.1**	2.6	2.4	**2.6**
HYB_DL	0.5	0.0	**104.4**	1.85	0.14	**1.99**	116.4	7.1	**123.5**	12.9	3.5	**16.4**	129.3	10.6	**139.9**	128.7	10.6	**139.3**	2.6	2.4	**2.6**
DBCLL_noAlk	0.5	0.0	**104.4**	1.94	0.04	**1.98**	124.4	2.0	**126.4**	13.2	0.9	**14.0**	137.6	2.9	**140.5**	137.0	2.9	**139.9**	2.6	2.5	**2.6**
DBCLL_duAlk	0.5	0.0	**104.4**	1.78	0.16	**1.94**	114.8	8.4	**123.1**	12.7	4.1	**16.8**	127.5	12.4	**139.9**	126.9	12.4	**139.3**	2.6	2.4	**2.5**
DBCLL_du-ssAlk	0.5	0.0	**104.4**	1.76	0.20	**1.96**	114.9	8.3	**123.2**	12.7	4.1	**16.8**	127.6	12.4	**140.0**	127.1	12.3	**139.4**	2.5	3.0	**2.6**
DBCLL_ClaqAlk	0.5	0.0	**104.4**	1.84	0.13	**1.97**	117.0	6.9	**123.8**	12.8	3.3	**16.1**	129.8	10.1	**139.9**	129.2	10.1	**139.3**	2.6	2.4	**2.6**
AeroCom	-	-	**122.0**	-	-	**1.80**	-	-	**140.0**	-	-	**14.3**	-	-	**154.3**	-	-	**151.0**	-	-	**4.5**
STD AeroCom	-	-	**±12.0**	-	-	**±0.81**	-	-	**±65.3**	-	-	**±163.3**	-	-	**±228.6**	-	-	**±56.0**	-	-	**±1.9**
GMI	-	-	**122.0**	-	-	**3.30**	-	-	**140.0**	-	-	**14.3**	-	-	**154.3**	-	-	**151.0**	-	-	**4.5**
EMAC 2008[1]	-	-	**138.0**	-	-	**1.90**	-	-	**302.0**	-	-	**504.0**	-	-	**806.0**	-	-	**187.0**	-	-	**0.9**
EMAC 2005-2008[2]	-	-	-	-	-	**1.78**	-	-	-	-	-	-	-	-	-	-	-	-	-	-	-
IFS[3]	-	-	**70.3**	-	-	**0.367**	-	-	**39.7**	-	-	**1.9**	-	-	**39.7**	-	-	**41.4**	-	-	**3.2**
LMDz-INCA	-	-	-	-	-	**1.26**	-	-	-	-	-	-	-	-	-	-	-	-	-	-	-
MetOffice UM[4]	-	-	-	-	-	-	-	-	-	-	-	-	-	-	-	-	-	-	-	-	-

1. From Bian et al. (2017).
2. From Karydis et al. (2016).
3. Fine NO_3^- reported from neutralization of nitric acid, ammonia and sulfate. Coarse nitrate from heterogeneous chemistry (Rémy et al., 2022).
4. Jones et al. (2021) performs two sensitivity tests to the accommodation coefficient used for NO_3^- formation in the fine mode: *FAST* with 0.193 and *SLOW* with 0.001. Here, results from the *FAST* test are reported on the basis that they present similar fine NO_3^- formation rates to our average fine nitrate results

Table S13. Nitrogen burdens (TgN) for each experiment and species.

Nitrogen burdens	**noHC**	**fTEQ noAlk**	**fTEQ du-ssAlk**	**HYB duUPTK**	**HYB du-ssUPTK**	**HYB gDU=0.1**	**HYB DL**	**DBCLL noAlk**	**DBCLL duAlk**	**DBCLL du-ssAlk**	**DBCLL ClaqAlk**
$HNO_{3(g)}$	1.06	1.11	0.65	0.44	0.15	0.1	0.16	1.14	0.6	0.56	0.57
$NH_{3(g)}$	0.71	0.04	0.13	0.17	0.21	0.23	0.31	0.05	0.11	0.28	0.25
$NO_{(g)}$	0.14	0.18	0.14	0.13	0.11	0.1	0.11	0.19	0.14	0.14	0.14
$NO_{2(g)}$	0.24	0.27	0.22	0.2	0.17	0.17	0.17	0.28	0.22	0.22	0.22
$N_2O_{5(g)}$	0.04	0.03	0.02	0.02	0.01	0.01	0.01	0.03	0.02	0.02	0.02
$NTR_{(g)}$	0.44	0.47	0.48	0.48	0.47	0.47	0.47	0.47	0.47	0.48	0.48
$PNA_{(g)}$	0.04	0.03	0.02	0.02	0.02	0.02	0.02	0.03	0.02	0.02	0.02
$PAN_{(g)}$	0.8	0.64	0.53	0.49	0.42	0.41	0.42	0.65	0.52	0.52	0.52
$PAN_{x(g)}$	0.16	0.13	0.11	0.11	0.09	0.09	0.09	0.14	0.11	0.11	0.11
$PM_{2.5}NO_{3(aer)}$	0	0.02	0.15	0.13	0.12	0.11	0.09	0.01	0.22	0.06	0.09
$PM_{2.5-10}NO_{3(aer)}$	0	0	0	0.13	0.27	0.32	0.29	0	0.11	0.18	0.14
$PM_{2.5}NH_{4(aer)}$	0	0.23	0.17	0.16	0.15	0.15	0.15	0.22	0.24	0.16	0.17
$PM_{2.5-10}NH_{4(aer)}$	0	0	0	0	0	0	0	0.01	0.01	0.01	0.01
$NO_{(g)}$ + $NO_{2(g)}$ + $NO_{3(g)}$	**0.39**	**0.46**	**0.36**	**0.33**	**0.28**	**0.28**	**0.28**	**0.47**	**0.37**	**0.36**	**0.36**
$NTR_{(g)}$ + $PNA_{(g)}$ + $PAN_{(g)}$ + $PAN_{x(g)}$	**1.44**	**1.28**	**1.14**	**1.09**	**1.01**	**0.99**	**1**	**1.29**	**1.13**	**1.13**	**1.13**
Aerosol nitrate + ammonium	**0**	**0.25**	**0.31**	**0.42**	**0.55**	**0.58**	**0.53**	**0.24**	**0.57**	**0.41**	**0.42**
Total nitrogen	**3.63**	**3.15**	**2.62**	**2.48**	**2.19**	**2.18**	**2.29**	**3.22**	**2.79**	**2.76**	**2.74**

S5 Discussion of additional sensitivity experiments

S5.1 HYB_g0p1

To assess the sensitivity to more efficient coarse NO_3^- production rates on dust (reaction R4 in Table 1), we perform the HYB_g0p1 run, that employs a constant value for γ_{dust} of 0.1, rather than utilizing the RH-dependent function proposed by (Fairlie et al., 2010). This experiment is also intended to elucidate the relative role of the dust over SS since, as noted in Section 2.2.1 , the γ_{dust} values used in both HYB_duUPTK and HYB_du-ssUPTK runs are well below the value used for γ_{SS} and other studies in the literature (Hauglustaine et al., 2014; Rémy et al., 2022). Results indicate an increase in coarse NO_3^- formation in regions rich in dust (Fig. S10), such as the Sahara desert, the Persian Gulf and East Asia (Fig. S3c). Furthermore, a slight enhancement in the transport of coarse NO_3^- across northern latitudes is observed, despite lower dust concentrations in that region. This can be attributed to the predominant production of coarse NO_3^- on dust across continental Eurasia, followed by its long-range transport at high altitudes to North America.

Among the mechanisms analyzed, HYB_g0p1 shows the most efficient depletion of $HNO_{3(g)}$, achieved by using a constant value of $\gamma = 0.1$ instead of the RH-dependent dust uptake coefficient from Fairlie et al. (2010). In this scenario, $HNO_{3(g)}$ is further reduced to 0.46 TgN, accompanied by an increase in coarse NO_3^- formation up to 1.93 Tg. Furthermore, the deposition rates rise from 140 to 149 Tg/y, as shown in Table 5 in the main text.

S5.2 DBCLL_duAlk

The DBCLL_duAlk configuration only accounts for dust alkalinity in the DBCLL mechanism. It shows that the sole presence of dust, compared to the case with no alkalinity in the DBCLL_noAlk configuration, significantly increases pH values (i.e. more basic) over the Sahara and continental Asia to a range of 6 to 8 (Fig. 4 g1, g2). Thereby, dust enhances the formation of both fine and coarse NO_3^- as well as coarse SO_4^{2-} in these regions. Additionally, fine NO_3^- formation is amplified in polluted areas, with surface concentrations rising beyond 5 $\mu g\ m^{-3}$ (an increase of 2-5 $\mu g\ m^{-3}$ relative to DBCLL_noAlk). This enhanced formation extends to regions rich in coarse dust, such as the Persian Gulf (surface concentrations of 1-3 $\mu g\ m^{-3}$) and central/downwind areas of the Saharan desert (surface concentrations of 0.2-0.5 $\mu g\ m^{-3}$ and loads of 2.0 $mg\ m^{-2}$), as shown in Figures 3 u and S1u. Over these areas, DBCLL_duAlk nearly depletes $HNO_{3(g)}$ gas (remaining surface concentrations of 0.01 to 0.05 $\mu g\ m^{-3}$). At high altitudes, both fine and coarse NO_3^- are distributed across the Atlantic and Pacific oceans with column loads of 1-2 $mg\ m^{-2}$ (Fig. S1u), resembling the transoceanic patterns also observed in the HYB mechanisms. Conversely, compared to the DBCLL_noAlk run, fine NH_4^+ increases over Europe and North-Central America (by at least 1 $mg\ m^{-2}$, discussed in Section 3.3.1), while it decreases over dusty areas (by 1.0 to 2.0 $mg\ m^{-2}$, Fig. S5t, q). This pattern is consistent with the comparison between the fTEQ_noAlk and the fTEQ_du-ssAlk runs (Fig. S5h, e). Concurrently, coarse NH_4^+ formation increases significantly in transoceanic areas, reaching 0.08-0.1 $mg\ m^{-2}$ alongside coarse NO_3^- particles, although its formation is halted over dusty regions (i.e. Middle East and Sahara, Fig. S5u). This inhibition can be attributed to the increased alkalinity of dust, which neutralizes $HNO_{3(g)}$ and limits the condensation of $NH_{3(g)}$. Lastly, the introduction of dust alkalinity strongly enhances the formation of coarse SO_4^{2-}, both over polluted regions (5 $mg\ m^{-2}$) and remote areas (0.2-

1.0 $mg\ m^{-2}$), as shown in Fig. S8. The enhanced production of coarse particles (principally coarse NO_3^-) provides additional surface area for $H_2SO_{4(g)}$ to condense on.

When compared with observations, DBCLL_duAlk results in opposite results to DBCLL_noAlk: $HNO_{3(g)}$ is underestimated with respect to observations from March to September by -0.1$\mu g\ m^{-3}$, while both fine and total particulate NO_3^- are overestimated with respect to observations by 1.5 and 2 $\mu g\ m^{-3}$ respectively (see Fig. S14).

Comparing the obtained NO_3^- burdens and size distributions with those reported by Rémy et al. (2022), Hauglustaine et al. (2014), and Jones et al. (2021) (Table 5), we observe that the total NO_3^- values are notably high when only dust alkalinity is considered. This discrepancy can be attributed to excessive fine NO_3^- formation, as already noted in the observational evaluation. This indicates that while the DBCLL_duAl approach improves the representation of alkalinity effects compared to the irreversible mechanisms, it still tends to overestimate the fine mode NO_3^-, suggesting a need for further refinement in the parameterization of NVC effects to achieve more accurate nitrate aerosol predictions. Moreover, deposition rates of total NO_3^- (54.01 Tg/y) fall below those reported by all the consulted references, suggesting that DBCLL_duAlk might form too much fine nitrate (with lower deposition rates) and misses coarse NO_3^- formation (with higher deposition rates).

S5.3 DBCLL_ClaqAlk

The DBCLL_ClaqAlk employs the average alkalinity of dust from Claquin et al. (1999) instead of Journet et al. (2014) with the DBCLL mechanism, and it shows significant differences in specific arid regions compared with DBCLL_du-ssAlk. Notably, with DBCLL_ClaqAlk the load of NO_3^- substantially increases over the Middle East and northern India, while a slight reduction is observed over northern Africa. These changes are significant enough to impact the long-range transport of both fine and coarse NO_3^- across the northern hemisphere (Fig. S3k, l). Coarse NO_3^- decreases by about 1-2 $mg\ m^{-2}$ over and downwind of dusty areas, while fine NO_3^- increases by 2-5 $mg\ m^{-2}$ along the equatorial belt and over polluted regions. Similar differences are found in particulate NH_4^+, although with an order of magnitude lower. Notably, $HNO_{3(g)}$ distributions report negligible differences between both runs. The lower alkalinity derived from the Claquin et al. (1999) dataset accounts for these differences, primarily affecting the formation of NO_3^- during long-range transport of dust,as discussed in Section 3.4 .

S6 Observational evaluation of oxidized and reduced species

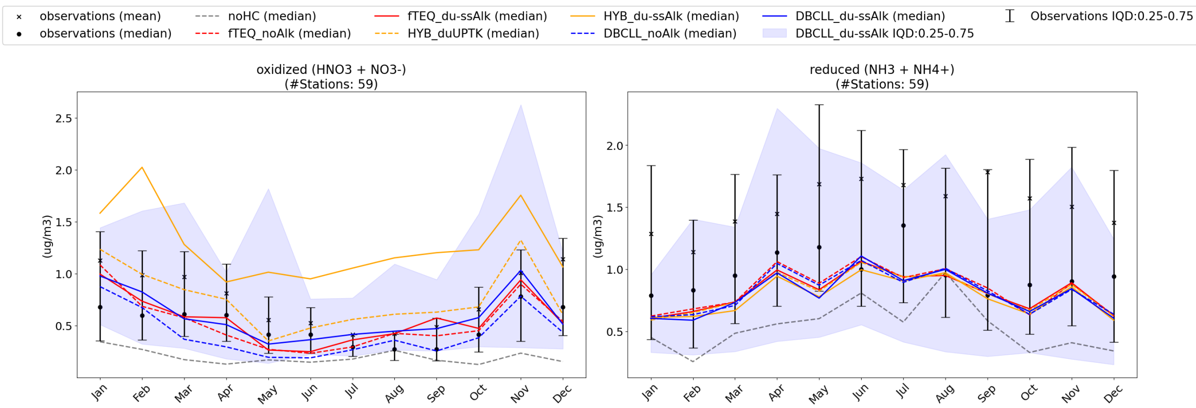

Figure S15. Observational evaluation for oxidized ($HNO_{3(g)}$ + NO_3^-, left) and reduced ($NH_{3(g)}$ + NH_4^+, right) nitrogen species.

Figure S16. Stations employed for the observational evaluation of oxidized ($HNO_{3(g)}$ + NO_3^-) and reduced ($NH_{3(g)}$ + NH_4^+) nitrogen species.

References

Bian, H., Chin, M., Hauglustaine, D. A., Schulz, M., Myhre, G., Bauer, S. E., Lund, M. T., Karydis, V. A., Kucsera, T. L., Pan, X., Pozzer, A., Skeie, R. B., Steenrod, S. D., Sudo, K., Tsigaridis, K., Tsimpidi, A. P., and Tsyro, S. G.: Investigation of global particulate nitrate from the AeroCom phase III experiment, Atmospheric Chemistry and Physics, 17, 12 911–12 940, https://doi.org/10.5194/acp-17-12911-2017, 2017.

Bleam, W.: Clay Mineralogy and Chemistry, Soil and Environmental Chemistry, pp. 87–146, https://doi.org/10.1016/B978-0-12-804178-9.00003-3, 2017.

Blum, A. E.: Feldspars in Weathering, pp. 595–630, Springer Netherlands, Dordrecht, https://doi.org/10.1007/978-94-011-1106-5_15, 1994.

Britannica, The Editors of Encyclopaedia: chlorite, https://www.britannica.com/science/chlorite-mineral, [Online; accessed March 11, 2024], 2018.

Claquin, T., Schulz, M., and Balkanski, Y. J.: Modeling the mineralogy of atmospheric dust sources, Journal of Geophysical Research: Atmospheres, 104, 22 243–22 256, https://doi.org/10.1029/1999JD900416, 1999.

Essington, M. E., Nelson, J. B., and Holden, W. L.: Gibbsite and Goethite Solubility, Soil Science Society of America Journal, 69, 996–1008, https://doi.org/10.2136/SSSAJ2004.0287, 2005.

Fairlie, T. D., Jacob, D. J., Dibb, J. E., Alexander, B., Avery, M. A., van Donkelaar, A., and Zhang, L.: Impact of mineral dust on nitrate, sulfate, and ozone in transpacific Asian pollution plumes, Atmospheric Chemistry and Physics, 10, 3999–4012, https://doi.org/10.5194/acp-10-3999-2010, 2010.

Hauglustaine, D. A., Balkanski, Y., and Schulz, M.: A global model simulation of present and future nitrate aerosols and their direct radiative forcing of climate, Atmospheric Chemistry and Physics, 14, 11 031–11 063, https://doi.org/10.5194/acp-14-11031-2014, 2014.

Hodzic, A., Bessagnet, B., and Vautard, R.: A model evaluation of coarse-mode nitrate heterogeneous formation on dust particles, Atmospheric Environment, 40, 4158–4171, https://doi.org/10.1016/j.atmosenv.2006.02.015, 2006.

Huggett, J.: Clay Minerals, Reference Module in Earth Systems and Environmental Sciences, https://doi.org/10.1016/B978-0-12-409548-9.09519-1, 2015.

Hulett, G. A. and Allen, L. E.: The solubility of gypsum, Journal of the American Chemical Society, 24, 667–679, https://doi.org/10.1021/JA02021A007/ASSET/JA02021A007.FP.PNG_V03, 1902.

Jones, A. C., Hill, A., Remy, S., Abraham, N. L., Dalvi, M., Hardacre, C., Hewitt, A. J., Johnson, B., Mulcahy, J. P., and Turnock, S. T.: Exploring the sensitivity of atmospheric nitrate concentrations to nitric acid uptake rate using the Met Office ' s Unified Model, Atmospheric Chemistry and Physics, 21, 1–48, https://doi.org/10.5194/acp-21-15901-2021, 2021.

Journet, E., Balkanski, Y., and Harrison, S. P.: A new data set of soil mineralogy for dust-cycle modeling, Atmospheric Chemistry and Physics, 14, 3801–3816, https://doi.org/10.5194/ACP-14-3801-2014, 2014.

Karydis, V. A., Tsimpidi, A. P., Pozzer, A., Astitha, M., and Lelieveld, J.: Effects of mineral dust on global atmospheric nitrate concentrations, Atmospheric Chemistry and Physics, 16, 1491–1509, https://doi.org/10.5194/acp-16-1491-2016, 2016.

Krueger, B. J., Grassian, V. H., Cowin, J. P., and Laskin, A.: Heterogeneous chemistry of individual mineral dust particles from different dust source regions: The importance of particle mineralogy, Atmospheric Environment, 38, 6253–6261, https://doi.org/10.1016/j.atmosenv.2004.07.010, 2004.

Mindat.org: Chlorite Group, https://www.Mindat.org/min-1016.html, [Online; accessed March 11, 2024], a.

Mindat.org: Feldspar Group, https://www.Mindat.org/min-1624.html, [Online; accessed March 11, 2024], b.

National Center for Biotechnology Information: PubChem Compound Summary for CID 14833, Hematite, https://pubchem.ncbi.nlm.nih.gov/compound/Hematite, [Online; accessed January 24, 2024], 2024a.

National Center for Biotechnology Information: PubChem Compound Summary for CID 92027383, Muscovite, https://pubchem.ncbi.nlm.nih.gov/compound/Muscovite, [Online; accessed January 24, 2024], 2024b.

National Center for Biotechnology Information. PubChem Compound Database: PubChem Compound Summary for CID 24928, Calcium Sulfate Dihydrate, https://pubchem.ncbi.nlm.nih.gov/compound/Calcium-Sulfate-Dihydrate, [Online; accessed January 24, 2024], 2024a.

National Center for Biotechnology Information. PubChem Compound Database: PubChem Compound Summary for CID 91502, Goethite (Fe(OH)O), https://pubchem.ncbi.nlm.nih.gov/compound/Goethite-_Fe_OH_O, [Online; accessed January 24, 2024], 2024b.

Nutting, P.: The solution and colloidal dispersion of minerals in water on JSTOR, Washington Academy of Sciences, 22, 261–267, https://www.jstor.org/stable/24522222, 1932.

Nutting, P. G.: THE ACTION OF SOME AQUEOUS SOLUTIONS ON CLAYS OF THE MONTMORILLONITE GROUP, UNITED STATES DEPARTMENT OF THE INTERIOR, pp. 219–235, 1941.

Rémy, S., Kipling, Z., Huijnen, V., Flemming, J., Nabat, P., Michou, M., Ades, M., Engelen, R., and Peuch, V. H.: Description and evaluation of the tropospheric aerosol scheme in the Integrated Forecasting System (IFS-AER, cycle 47R1) of ECMWF, Geoscientific Model Development, 15, 4881–4912, https://doi.org/10.5194/gmd-15-4881-2022, 2022.

Schulze, D. G.: CLAY MINERALS, Encyclopedia of Soils in the Environment, 4, 246–254, https://doi.org/10.1016/B0-12-348530-4/00189-2, 2005.

Usher, C. R., Michel, A. E., and Grassian, V. H.: Reactions on Mineral Dust, Chemical Reviews, 103, 4883–4939, https://doi.org/10.1021/cr020657y, 2003.

Weast, R. C.: CRC Handbook of Chemistry and Physics, Cronus Books, 60 edn., https://www.abebooks.com/servlet/BookDetailsPL?bi=31210018960&searchurl=an%3Dweast%2Brobert%26sortby%3D17%26tn%3Dcrc%2Bhandbook%2Bchemistry%2Bphysics%2B60th&cm_sp=snippet-_-srp1-_-title1, 1980.

Webmineral: Albite Mineral Data, http://webmineral.com/data/Albite.shtml, [Online; accessed 11 March 2024], 2008a.

Webmineral: Anorthite Mineral Data, http://webmineral.com/data/Anorthite.shtml, [Online; accessed 11 March 2024], 2008b.

Webmineral: Calcite Mineral Data, http://webmineral.com/data/Calcite.shtml, [Online; accessed 11 March 2024], 2008c.

Webmineral: Gypsum Mineral Data, http://webmineral.com/data/Gypsum.shtml, [Online; accessed 11 March 2024], 2008d.

Webmineral: Orthoclase Mineral Data, http://webmineral.com/data/Orthoclase.shtml, [Online; accessed 11 March 2024], 2008e.

Webmineral: Illite Mineral Data, http://webmineral.com/data/Illite.shtml, [Online; accessed 20 October 2022], 2008f.

Yang, L.: Title Kaolinite dissolution and precipitation kinetics at 22oC and pH 4 Permalink https://escholarship.org/uc/item/0qz871kp Publication Date, https://escholarship.org/uc/item/0qz871kp, 2008.

Zhang, Y. and Muhammed, M.: Solubility of Calcium Sulfate Dihydrate in Nitric Acid Solutions Containing Calcium Nitrate and Phosphoric Acid, Journal of Chemical and Engineering Data, 34, 121–124, https://doi.org/10.1021/je00055a032, 1989.